JOURNAL OF MAGNETIC RESONANCE **132,** 220–239 (1998)
ARTICLE NO. MN981427

Computation of Orientational Averages in Solid-State NMR by Gaussian Spherical Quadrature

Mattias Edén[1] and Malcolm H. Levitt

Physical Chemistry Division, Arrhenius Laboratory, Stockholm University, S-106 91 Stockholm, Sweden

Received November 17, 1997; revised February 27, 1998

We investigate Gaussian spherical quadrature as a method for calculating orientational averages in solid-state NMR. For the case of magic-angle-spinning sideband amplitudes of isolated spins-1/2, we demonstrate the superiority of Gaussian spherical quadrature over other orientational averaging methods. Depending on the shift anisotropy parameters and the desired accuracy, the computation speed is enhanced by a large factor (between two and many hundreds). In addition, a method for improving any present sampling scheme is devised. Such schemes are called SHREWD (Spherical Harmonic Reduction or Elimination by a Weighted Distribution). The role of orientational symmetry in solid-state NMR is explored. We also discuss the limitations of the Gaussian spherical quadrature methods.

Key Words: **solid-state NMR; magic-angle-spinning; powder average; orientational symmetry; Gaussian spherical quadrature.**

INTRODUCTION

Solid-state NMR is a powerful method for obtaining geometrical and dynamical information at the molecular level. As opposed to liquid-state NMR, the *anisotropic* spin interactions are directly accessible. The magnitude and direction of these interactions are closely linked to the local molecular structure. For example, the through-space dipole–dipole coupling is directly related to the distance between nuclei and the bond directions. Recently developed experiments allow estimation of internuclear distances (*1–3*) and molecular torsional and interbond angles (*4–7*), even in biomolecules with high molecular weights.

Solid-state NMR methods are often applied to systems with no long-range molecular order, such as powders, polycrystalline materials, most polymers, and amorphous materials. The NMR response of nonoriented samples is a superposition of signals from very many molecular orientations. In most cases, the NMR signal cannot be derived analytically and must be calculated numerically. The numerical simulation must therefore incorporate a ''powder average'' over all possible molecular orientations. Since the computation of the NMR signal for each orientation is often time-consuming, it is highly desirable that a reasonable numerical approximation to a full powder average be obtained using a minimum number of orientational samples.

[1] Corresponding author: mattias@physc.su.se.

This raises the issue of how to select the molecular orientations used in the simulation. The most obvious scheme is simply to generate the orientational samples randomly, so as to emulate the physical situation in a real unoriented sample. Unfortunately, a real powder consists of an enormous number of orientations—for example, 100 μl powder in which each crystallite consists of a cube with side 10 μm contains 10^8 separate crystallites. Usually, it is out of the question to simulate such a large number of orientations.

A random sampling scheme performs poorly if the number of orientational samples is reduced to a few hundred. This is because thinly distributed random values tend to form ''clumps''—a well-known example is the formation of constellations of stars in the night sky. Improved sampling strategies tend to concentrate on reducing the ''clumping'' as much as possible, by ensuring that the orientational samples are evenly distributed. Normally, geometrical arguments are used to distribute the orientational samples as evenly as possible (like the placement of dimples on the surface of a golf ball (*8*)). We refer to such approaches as ''geometrical.''

In this article we stress a different approach, which is ''mathematical'' rather than ''geometrical'' in essence. The method is based on an assumption that the function to be averaged may be expressed accurately as a finite series of orthogonal functions, where each function is multiplied by an (unknown) coefficient. One of these coefficients is the accurate average of the function. The orientational samples are then selected so that a large number of the remaining functions are eliminated identically, leaving only the target coefficient: the orientational average. The most important schemes of this type were developed by Lebedev (*9–12*). The Lebedev schemes are widely used in other branches of science, especially in density functional theory (*13–15*). We show here that they have significant advantages for some problems in solid-state NMR as well.

The design of optimal orientational sampling schemes depend greatly on the *symmetry* of the function to be averaged with respect to the orientational variable. The Lebedev schemes appear to be particularly suitable when the averaged function displays some kind of orientational symmetry. One section of this article attempts to classify solid-state NMR problems in terms of the symmetry they display.

1090-7807/98 $25.00

ORIENTATIONAL AVERAGING

Euler Angles and Reference Frames

In general, numerical calculations of solid-state NMR signals involve the calculation of an orientationally dependent function $f(\Omega)$, where the orientation Ω may conveniently be expressed as an Euler angle triplet $\Omega = (\alpha, \beta, \gamma)$ (*16*). The function may also depend on other parameters as well, not indicated explicitly here. The Euler angles $\Omega = (\alpha, \beta, \gamma)$ represent the relationship between two different reference frames.

The proper choice of these reference frames depends on the problem. For example, in rotating solids, Ω refers to the relationship between a molecular reference frame *M*, fixed with respect to the molecular framework, and a rotor-reference frame *R*, fixed with respect to the rotating sample holder (''rotor''). The Euler angles are then notated $\Omega_{MR} = (\alpha_{MR}, \beta_{MR}, \gamma_{MR})$. In static solids, it is usually more appropriate to choose a ''laboratory'' reference frame *L*, fixed with respect to the applied magnetic field. In this case the Euler angles are notated $\Omega_{ML} = (\alpha_{ML}, \beta_{ML}, \gamma_{ML})$.

In all cases, the key points are (i) the orientational angles Ω_{MR} or Ω_{ML} are time-independent over the duration of the experiment, and (ii) the actual physical situation may be represented accurately by an integration over all possible values of the orientational variable. For example, in a rotating solid it would be inappropriate to use Ω_{ML} as a variable, because these Euler angles are time-dependent.

If the NMR spin dynamics depend only on a single anisotropic interaction Λ, it is possible to choose the molecular frame to coincide with the principal axis system (PAS) of Λ, denoted P^{Λ}. The relevant orientational variable is then written Ω^{Λ}_{PR} (for rotating solids) or Ω^{Λ}_{PL} (for static solids). The number of sampled orientations may be considerably reduced in this case, as discussed later.

In the following discussion, the variable Ω is used to refer to the appropriate variable Ω_{MR}, Ω_{RL}, Ω^{Λ}_{PR} or Ω^{Λ}_{PL}, depending on the problem.

Orientational Averaging—the General Case

The orientational average of f corresponds to the integral

$$\bar{f} = \mathcal{N}^{(3)} \int_{V^{(3)}} f(\Omega)\, d\Omega, \qquad [1]$$

where the volume of integration $V^{(3)}$ represents the ranges for the three Euler angles,

$$V^{(3)} = \{0 \le \alpha < 2\pi,\ 0 \le \beta \le \pi,\ 0 \le \gamma < 2\pi\}$$
$$d\Omega = \sin\beta\ d\alpha\ d\beta\ d\gamma, \qquad [2]$$

and the normalization constant is

$$\mathcal{N}^{(3)} = (8\pi^2)^{-1}. \qquad [3]$$

In numerical calculations, this integral is approximated by summing the function over a set of N^S different orientations and weights $S = \{w_j^S, \Omega_j^S\}$,

$$\bar{f}^S = \sum_{j=1}^{N^S} w_j^S f(\Omega_j^S), \qquad [4]$$

where the weights are normalized so that their sum equals unity. $\bar{f}^S$ is the *estimate* of the powder average $\bar{f}$, using the sampling scheme *S*. The optimum sampling scheme *S* for a given number of samples N^S minimizes the error of integration ϵ^S, defined by

$$\epsilon^S = |\bar{f} - \bar{f}^S|. \qquad [5]$$

Two-Angle Integration

In many important cases, it is not necessary to perform the integration over the angle γ explicitly. Either the function f is independent of γ, or the average over γ may be performed implicitly by a modification of the function itself (*17–19*). Some examples are given later. In these cases, the orientational averaging of the function reduces to a *two-angle integration*, specified by

$$\bar{f} = \mathcal{N}^{(2)} \int_{V^{(2)}} f(\Omega)\, d\Omega, \qquad [6]$$

where

$$V^{(2)} = \{0 \le \alpha < 2\pi,\ 0 \le \beta \le \pi\}$$
$$d\Omega = \sin\beta\ d\alpha\ d\beta$$
$$\mathcal{N}^{(2)} = (4\pi)^{-1}. \qquad [7]$$

In this case, it is possible to use the following relationship between the two Euler angles (α, β) and the polar angles (θ, ϕ): $\theta \equiv \beta$ and $\phi \equiv \alpha$. The two-angle orientational average is equivalent to the integration of a function on the surface of a sphere, a property which is exploited in the ''geometrical'' sampling approaches.

The conditions under which the orientational averaging may be reduced from three angles to two angles are investigated later.

Most of the following discussion is restricted to the problem of two-angle orientational averaging.

Existing Powder Averaging Methods

A large number of powder averaging methods have been reported (*20–30*). In Ref. (*25*), many methods were compared. In the following discussion, we focus on those methods which were reported to give best results, as well as the commonly used ''step method.'' The schemes evaluated in this article are specified completely in Appendix 1.

(i) The *step* method: The simplest version of this approach divides each of the α- and β-ranges (and γ when appropriate) into evenly spaced meshes. The weights w_j^S are proportional to $\sin \beta_j^S$.

(ii) The *ZCW* sampling schemes were originated by Zaremba (*26*) and later modified by Conroy (*27*) and Wolfsberg and coworkers (*28*). These schemes are commonly used in solid-state NMR (*3, 29*). The orientations generated are solutions of Diophantine equations, and provide rather uniform distributions of orientations. The weights w_j^S are uniform in the ZCW method.

(iii) *REPULSION* (*25*). This elegant method takes the geometrical approach to its logical conclusion. A very even distribution of orientations is obtained by first placing N^S particles on the surface of a sphere, and then adjusting their positions while minimizing a repulsive potential function between each particle and its neighbors. The final stage of the optimization is to adjust the weights w_j^S according to the proximity of nearest neighbors to each sampling point.

A weak point in the REPULSION scheme is that the optimization of the weights w_j^S is rather arbitrary. We demonstrate below a new method for optimization of the weights.

GAUSSIAN SPHERICAL QUADRATURE

The basic idea behind a *Gaussian quadrature* (*31*) is that any function may be expanded as a sum of orthogonal basis functions, usually polynomials of increasing order L. If the expansion is convergent, and the coefficients are very small beyond a certain maximum rank $L_{\max}$, then the function can be approximated within a certain error by a truncated series using basis functions with $L \leq L_{\max}$. The average of the function is estimated by choosing the samples and weights so that all polynomials up to and including the order $L_{\max}$ are integrated as accurately as possible. Gaussian quadrature is extensively used in numerical integration (*31*) and has been applied explicitly to some NMR problems (*30, 32*).

For a two-angle spherical average, the appropriate polynomial functions are the spherical harmonics. This integration method is called a *Gaussian spherical quadrature*. Angle sets have been constructed that provide *exact* integration of spherical harmonics for all $L \leq L_{\max}$ with, presumably, the lowest possible number of angles for a given $L_{\max}$ (*9–12*).

The efficiency of this approach depends on the maximum order required for an accurate estimate of f; the lower the value of $L_{\max}$, the smaller N needs to be for exact integration.

Spherical Sampling Moments and Integration Errors

Consider first the general case requiring integration over all three Euler angles $\Omega = (\alpha, \beta, \gamma)$. The function $f(\Omega)$ may be expressed as an infinite sum of Wigner functions $D^L_{qq'}(\Omega)$:

$$f(\Omega) = \sum_{L=0}^{\infty} \sum_{q,q'=-L}^{L} f_{Lqq'} D^L_{qq'}(\Omega), \qquad [8]$$

where

$$D^L_{qq'}(\alpha, \beta, \gamma) = \exp\{-iq\alpha\} d_{qq'}(\beta) \exp\{-iq'\gamma\}, \qquad [9]$$

and $d_{qq'}(\beta)$ is a reduced Wigner function (*16*). The Wigner functions are orthogonal, meaning

$$\int_{V^{(3)}} D^L_{qq'}(\Omega)(D^{L'}_{q''q'''}(\Omega))^* d\Omega = \frac{8\pi^2}{2L+1} \delta_{LL'} \delta_{qq''} \delta_{q'q'''}, \qquad [10]$$

where the asterisk denotes complex conjugation and δ_{mn} is the Kronecker delta function. The Wigner functions have the following integral over $V^{(3)}$:

$$\int_{V^{(3)}} D^L_{qq'}(\Omega) d\Omega = 8\pi^2 \delta_{L0} \delta_{q0} \delta_{q'0}. \qquad [11]$$

It follows that the integral of f over $V^{(3)}$ evaluates to

$$\bar{f} = f_{000}. \qquad [12]$$

Hence, the orientational average of f corresponds to the expansion coefficient of $D^0_{00} = 1$. The purpose of powder averaging may be reinterpreted as ''projecting out'' this component from the infinite series.

In the following discussion, we assume that the series of coefficients $f_{Lqq'}$ is convergent and falls rapidly to zero for L larger than some threshold value $L^f_{\max}$. Roughly speaking, functions that are ''difficult'' to integrate have large values of $L^f_{\max}$, and functions which are ''easy'' to integrate have small values of $L^f_{\max}$.

The characteristics of a sampling scheme may be stated in terms of its *sampling moments*, defined by

$$\sigma^S_{Lqq'} = \sum_{j=1}^{N^S} w_j^S D^L_{qq'}(\Omega_j^S). \qquad [13]$$

By definition, $\sigma^S_{000} = 1$. From the orthogonality of the Wigner functions, the estimated orientational average of the function, obtained by a given sampling scheme, is equal to

$$\bar{f}^S = \sum_{L=0}^{\infty} \sum_{q,q'=-L}^{L} f_{Lqq'} \sigma^S_{Lqq'}. \qquad [14]$$

The exact integral of the function is the first term in this series, so the error generated by the sampling scheme is

$$\epsilon^S = \left| \sum_{L=1}^{\infty} \sum_{q,q'=-L}^{L} f_{Lqq'} \sigma^S_{Lqq'} \right|. \qquad [15]$$

This represents the *overlap* between the spherical moments of the function $f_{Lqq'}$, and the sampling moments $\sigma^S_{Lqq'}$, for all ranks $L \geq 1$. Since $f_{Lqq'}$ is very small for $L > L^f_{\max}$, a scheme S provides an accurate estimate of the orientational average of f if the sampling moments $\sigma^S_{Lqq'}$ are small for all ranks L in the range $1 \leq L \leq L^f_{\max}$.

Rank Profiles

If the function depends only on the Euler angles α and β, the coefficients $f_{Lqq'}$ are zero for $q' \neq 0$, so that only the moments f_{Lq0} and σ^S_{Lq0} are relevant. It is convenient to use the following expressions for rms sampling moments and function coefficients:

$$\sigma^S_L = \left(\frac{1}{2L+1} \sum_{q=-L}^{L} |\sigma^S_{Lq0}|^2\right)^{1/2} \quad [16]$$

$$f_L = \left(\frac{1}{2L+1} \sum_{q=-L}^{L} |f_{Lq0}|^2\right)^{1/2}. \quad [17]$$

We call the plot of σ^S_L against L the *rank-profile* of a sampling scheme, and the plot of f_L against L the rank-profile of the function to be averaged. These rank-profiles give a good qualitative indication of the performance of a sampling scheme. An example of a rank-profile for a certain function is given in Fig. 1a. Rank profiles of two orientational sampling schemes are given in Figs. 1b and c. The scheme given in Fig. 1b is expected to be ''poor'' since there is significant overlap between the regions where f_L and σ^S_L are finite. The scheme in Fig. 1c is expected to be ''good'' because the moments σ^S_L are only significant in the region beyond $L > L^f_{\max}$.

The Lebedev Schemes

It is possible to design sampling schemes that integrate *all* spherical harmonics *exactly* up to and including a certain order $L^S_{\max}$. These schemes may be applied to the two-angle averaging problem because the Wigner function $D^L_{q0}(\alpha, \beta)$ is proportional to the spherical harmonic $Y_{Lq}(\beta, \alpha)$. Note here the distinction between $L^S_{\max}$, the maximum rank for which all sampling moments vanish for a certain Gaussian spherical quadrature *scheme*, and $L^f_{\max}$, which is the highest rank represented in the series expansion of the *function* to be integrated.

The schemes of Lebedev (*9–12*) are constructed under octahedral symmetry (O_h). The Lebedev schemes have the properties

$$\sigma^S_L = 0 \text{ for } 1 \leq L \leq L_{\max}$$
$$\sigma^S_L = 0 \text{ for } L \text{ odd} \quad [18]$$

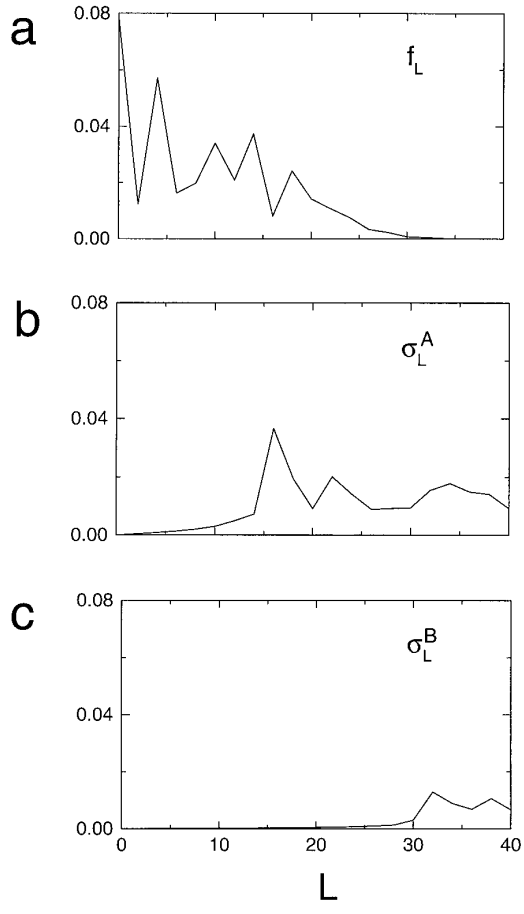

FIG. 1. (a) Rms expansion coefficients f_L plotted against rank. The coefficient f_0 is the orientational average $\bar{f}$. (b), (c) Rms sampling moments (σ^S_L) as function of rank for two schemes, A and B. The values $\sigma^S_0 = 1$ are not shown in plots b and c. Scheme A would give a poor estimation of $\bar{f}$, while scheme B would be accurate.

and are believed to perform this task in the minimum possible number of angles, given approximately by

$$N^S_{\text{LEB}} \simeq \frac{(L^S_{\max}+1)^2}{3}, \; L^S_{\max} \text{ odd}. \quad [19]$$

Lebedev schemes exist for a variety of $L^S_{\max}$ values, the largest reported so far being 53. The number of angles N^S_{LEB} for various values of $L^S_{\max}$ are given in Table 1. Since the octahedral group contains inversion, the angles come in pairs $(\alpha_2, \beta_2) = (\alpha_1 + \pi, \pi - \beta_1)$. This inversion symmetry on the sphere cancels identically the sampling moments σ^S_{Lq0} for all odd ranks L.

Figure 2 compares rank-profiles for some Lebedev sets with two schemes based on the geometrical approach. Note the completely flat profile of the Lebedev schemes out to the rank $L = L_{\max}$, and the ''sawtooth'' appearance of the sampling moments beyond that. The schemes ZCW and REPULSION do not set any of the sampling moments exactly equal to zero,

TABLE 1
The Number of Orientations Required in Spherical Quadrature Schemes

L^S_{max}	N(LEB)[a]	N(LEBhemi)[b]	N(LEBoct)[c]	N(SHREWD-STEPhemi)[b]	N(SHREWD-STEPoct)[c]
11	50	25	10	66	18
15	86	43	16	120	36
17	110	55	19	153	45
19	146	73	22	190	50
23	194	97	31	276	72
29	302	151	46	435	120
41	590	295	85	861	231
47	770	385	109	1128	288
60	—	—	—	1891	496
100	—	—	—	5151	1326

[a] All spherical harmonics with rank $L \leq L^S_{max}$ are eliminated, and also all odd L spherical harmonics.
[b] All spherical harmonics are eliminated whose rank L is both even and less than or equal to L^S_{max}.
[c] All real parts of spherical harmonics are eliminated whose rank L is both even and less than or equal to L^S_{max}, and whose q value is also even.

although the moments decrease gradually as the number of angles grows.

There is no strict correspondence between these rank profiles and the actual performance of an orientational sampling scheme. The error depends, as described earlier, on the rank profile for the function $f(\Omega)$ as well as that of the sampling scheme. For functions with convergent rank profiles, this implies that the error is largely determined by the performance at high ranks $L > L^f_{max}$, which has irregular behavior, as may be seen from these plots. Furthermore, the rank profiles obscure the phase relationship between the moments σ^S_{Lq0} with different q. Nevertheless, it is possible to draw some qualitative conclusions:

1. The perfectly flat rank profile of the Lebedev schemes at low L values allows these schemes to achieve extremely high accuracy using a relatively low number of sampling points. The Lebedev schemes are therefore greatly superior in cases where high accuracy is required, providing of course that the function is such that $L^f_{max} \leq 53$.

2. The situation is less clear when the goal is to achieve moderate accuracy of the powder average using a minimal number of orientational samples. In this case, a compromise must be achieved between performance at high and low ranks L. The Lebedev schemes generally have high sampling moments just beyond the threshold L^S_{max}, whereas the best ''geometrical'' schemes achieve a rather smooth profile with a broad

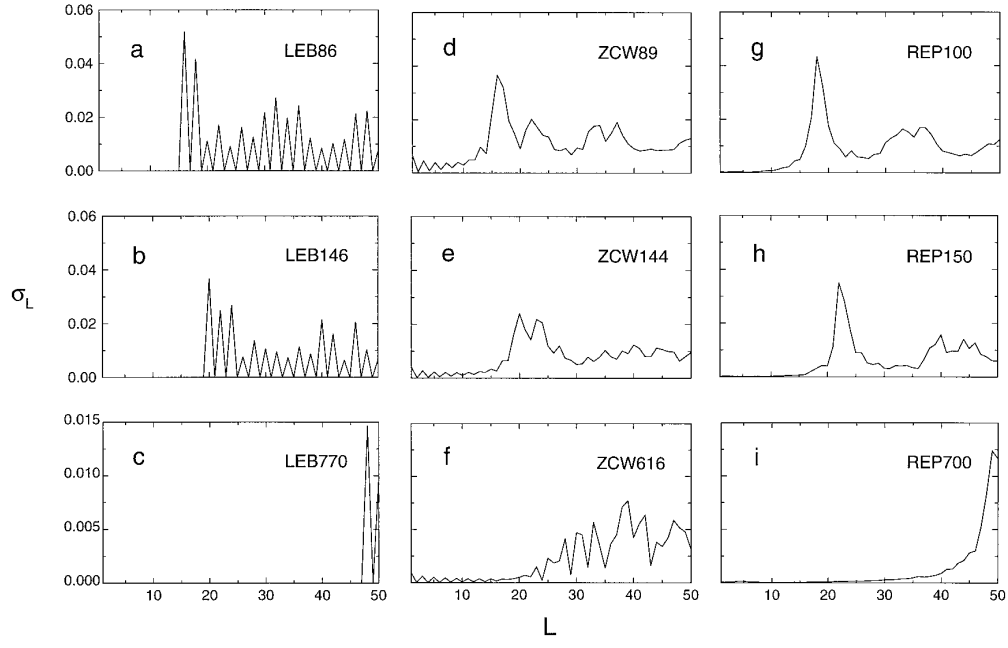

FIG. 2. Rms sampling moments σ^S_L for three powder methods at comparable numbers of angles. The moment $\sigma^S_0 = 1$ is not shown. The plots include Lebedev schemes with $L^S_{max} = 15$ (a), 19 (b), and 47 (c), ZCW schemes (d)–(f), and REPULSION sets (g)–(i). Note the magnified scale in the lower three plots.

flat region at low ranks, peaking more gradually. In applications which do not demand extremely high accuracy, other methods such as ZCW and REPULSION may therefore outperform the Lebedev schemes.

3. In many problems in solid-state NMR, the function $f(\Omega)$ possesses symmetry with respect to the orientation Ω. In these cases, the Lebedev schemes gain a further advantage over most of the ''geometrical'' schemes, because they are based upon octahedral symmetry, and the number of sampling points is readily reduced by large factors if the integrand possesses symmetry. This is not generally true for the ZCW and REPULSION schemes, which do not at the moment exploit orientational symmetry. In the next section, we discuss symmetry and its consequences for numerical calculation of powder averages.

ORIENTATIONAL SYMMETRY

The orientational symmetry of typical functions of interest in solid-state NMR is discussed in Appendix 2. The following orientational symmetries may be identified.

Three-Angle Dependence

For these problems, the function f displays in general no symmetry whatsoever with respect to the orientational variables $\Omega = (\alpha, \beta, \gamma)$. The most general cases in the NMR of rotating solids fall into this category.

Two-Angle Dependence: Symmetry Group C_i

For these problems, either the function to be averaged is independent of the Euler angle γ, or else the averaging over γ may be done implicitly by a simple modification of f. In addition, there is a further symmetry in (α, β) corresponding to inversion of points through the center of the sphere. These properties may be expressed

$$\begin{aligned} f(\alpha, \beta, \gamma) &= f(\alpha, \beta, 0) \\ f(\alpha, \beta, 0) &= f(\alpha + \pi, \pi - \beta, 0). \end{aligned} \quad [20]$$

Since inversion is the only symmetry element, the corresponding point symmetry group has the Schönflies symbol C_i. This symmetry leads to the following properties of the spherical components of f:

$$\begin{aligned} f_{Lqq'} &= f_{Lq0}\,\delta_{q'0} \\ f_{Lq0} &= 0 \text{ for odd } L. \end{aligned} \quad [21]$$

For problems of this type, a powder average may be computed by integrating f over a hemisphere $0 \le \alpha < 2\pi$, $0 \le \beta \le \pi/2$.

For problems with C_i symmetry, the relevant orientational sampling moments $\sigma_L^S(C_i)$ are given by Eq. [16] with L taking only even values.

All cases in the NMR of static solids, and many problems in the NMR of rotating solids, display C_i symmetry. As discussed in the appendix, the NMR signal from a rotating solid has C_i symmetry if (i) the eigenstates of the spin Hamiltonian do not change as the sample rotates, and (ii) the observable coherences are prepared with orientation-independent phases. The spinning sideband patterns generated by ''inhomogeneous'' interactions (in the dynamic sense of Maricq and Waugh (*33*)) display C_i symmetry with respect to molecular orientation.

Recently, we have proved that an important class of dynamically ''homogeneous'' problems also has C_i symmetry. This includes the NMR spectra of arbitrary coupled spin systems in rotating powdered solids, in the absence of radio-frequency fields, and with uniform preparation of the spin coherences. The conditions leading to C_i symmetry in dynamically ''homogeneous'' problems are discussed in a following paper (*34*).

Two-Angle Dependence: Symmetry Group D_{2h}

These problems display two additional properties in the function f:

$$\begin{aligned} f(\pi + \alpha, \beta, 0) &= f(\alpha, \beta, 0) \\ f(-\alpha, \beta, 0) &= f(\alpha, \beta, 0). \end{aligned} \quad [22]$$

On the unit sphere, these correspond to a twofold rotation axis along z and a reflection plane xz. Combined with the inversion operation, the function conforms to symmetry group D_{2h}. The corresponding properties of the spherical coefficients are

$$\begin{aligned} f_{Lqq'} &= f_{Lq0}\,\delta_{q'0} \\ f_{Lq0} &= 0 \text{ for odd } L \\ f_{Lq0} &= 0 \text{ for odd } q \\ f_{Lq0} &= f^*_{Lq0}. \end{aligned} \quad [23]$$

For problems of type D_{2h}, it is only necessary to integrate over one octant of the sphere: $0 \le \alpha \le \pi/2$, $0 \le \beta \le \pi/2$. This case is common if there is only one anisotropic spin interaction involved and the orientational scheme exploits the principal axis system of that interaction. D_{2h} symmetry is also encountered if there are several interactions, all sharing the same principal axis frame.

For problems with D_{2h} symmetry, the relevant sampling moments may be defined through

$$\sigma_L^S(\mathrm{D_{2h}}) = \left(\frac{1}{\mathrm{L}+1} \sum_{\substack{\mathrm{q}=-L, \\ q \text{ even}}}^{L} |\mathrm{Re}\{\sigma_{Lq0}^S\}|^2\right)^{1/2},\ L \text{ even}. \quad [24]$$

For *static solids in high field*, the existence of a single anisotropic interaction, or several interactions with common reference frames, is sufficient to establish D_{2h} symmetry (*35*).

For *rotating solids in high field*, one needs in general (i) a single anisotropic interaction, or several interactions with common principal axis frames; (ii) time-independent eigenstates of

the spin Hamiltonian; (iii) observable coherences excited with orientation-independent phases. An important example in rotating solids is the generation of spinning sidebands by the chemical shift anisotropy interaction of isolated spin sites, as discussed later.

Other Forms of Symmetry

Other forms of orientational symmetry appear to be rare. For example, we are aware of no cases in which the function is independent of γ, but for which the equivalence of $f(\alpha, \beta)$ and $f(\pi + \alpha, \pi - \beta)$ cannot be established. Cases in which $f(\alpha, \beta, 0)$ is equal to $f(\pi + \alpha, \beta, 0)$ but not to $f(-\alpha, \beta, 0)$ appear to be equally rare.

EXPLOITATION OF SYMMETRY

Two-Angle Dependence

Orientational symmetry has a major effect on the computation of powder averages. The Lebedev schemes belong to the O_h symmetry group, which contains both C_i and D_{2h} as subgroups. If an angle pair (α, β) is a member of a Lebedev set, then either the seven angle pairs

$$(\pi + \alpha, \beta); (-\alpha, \beta); (\pi - \alpha, \beta); (\alpha, \pi - \beta);$$
$$(\pi + \alpha, \pi - \beta); (-\alpha, \pi - \beta); (\pi - \alpha, \pi - \beta) \quad [25]$$

are also included in the Lebedev set, or else one of them *coincides* with (α, β), within modulo 2π. Clearly, computation may be restricted to those pairs which are not related by the symmetry operations of the appropriate group. These symmetry reductions give the Lebedev sets a decisive advantage for problems of types C_i and D_{2h}.

For problems of type C_i, the Lebedev angle sets may be reduced by a factor of 2. The angle pairs in the reduced set may be constrained to the upper hemisphere of the sphere. For this reason, we refer to this type of Lebedev set as a *hemispherical Lebedev* set, denoted LEBhemi*N*, where *N* is the number of orientations in the set.

For problems of type D_{2h}, the Lebedev sets may be reduced by a factor between 5 and 8. The angles may be constrained to a single octant of the sphere. Such sets are called here *octant Lebedev* sets and denoted LEBoct*N*.

The number of angles in the reduced Lebedev sets are listed in Table 1, and a scheme is given explicitly in Table 2.

It is also possible to construct ''geometrical'' schemes with symmetrical distributions of sampling points. Two examples are the step method and SOPHE (*23*). These angle sets may also be reduced by large factors when applied to problems of type C_i and D_{2h}.

Many schemes, such as the current versions of ZCW and REPULSION, cannot be reduced under C_i or D_{2h} symmetry. Nevertheless, the symmetry of the integrand may still be exploited by distributing the points over only one half of the sphere (*20, 29*) (in the case of C_i symmetry), or over only one octant of the sphere (in the case of D_{2h} symmetry). This leads to a higher density of sampling points, which is expected to improve the accuracy of the integration. Our implementation of this for ZCW is described in Appendix 1. In practice, we often found the improvement in performance rather marginal. However, it is possible to improve performance further by optimizing the weights w_j^S, as described in the next section. REPULSION may also be adapted to the symmetry of the integrand by building symmetry constraints into the pseudopotential used in optimizing the angle sets. For example, each point could be associated with symmetry-related ''images'' (*25*). At the moment, it is not known whether symmetrized REPULSION sets are competitive with the Lebedev schemes.

TABLE 2
Orientations and Weights for LEBoct31

α	β	w
0.00000000	0.00000000	0.003564681
0.00000000	20.2288199	0.020207384
0.00000000	45.0000000	0.022867624
0.00000000	69.7711801	0.020207384
0.00000000	90.0000000	0.003564681
7.52995108	82.5342479	0.032854216
10.7708560	58.3237741	0.044241991
16.8498911	33.2761302	0.044241991
17.5875412	73.1871458	0.041265902
20.2288199	90.0000000	0.020207384
25.0816830	47.8327264	0.044869633
29.7677350	63.5962810	0.044150172
32.1331436	80.8487219	0.044241991
45.0000000	10.5884838	0.032854216
45.0000000	24.1455738	0.041265902
45.0000000	38.9683735	0.044150172
45.0000000	54.7356103	0.044587065
45.0000000	71.6876561	0.044869633
45.0000000	90.0000000	0.022867624
57.8668563	80.8487219	0.044241991
60.2322650	63.5962810	0.044150172
64.9183170	47.8327264	0.044869633
69.7711801	90.0000000	0.020207384
72.4124588	73.1871458	0.041265902
73.1501089	33.2761302	0.044241991
79.2291440	58.3237741	0.044241991
82.4700489	82.5342479	0.032854216
90.0000000	20.2288199	0.020207384
90.0000000	45.0000000	0.022867624
90.0000000	69.7711801	0.020207384
90.0000000	90.0000000	0.003564681

Note. Orientations in degrees.

Three-Angle Dependence

In the NMR of rotating solids, the function to be evaluated often has no symmetry at all in the orientational variables. A three-angle average must be computed. The Lebedev sets apply only to two-angle averaging and cannot be used directly. This

also applies to many other schemes treated here, such as REPULSION.

Any two-angle scheme may be extended to the three-angle case by handling the γ-angle separately. For example, all $D^L_{qq'}(\Omega)$ for $L \leq L_{\max}$ may be integrated exactly by combining a Lebedev method with a $(L_{\max} + 1)$-fold step in the γ-range. However, this requires a large number of angles and is probably far from optimal.

The Lebedev sets may presumably be generalized to produce accurate quadratures of the three-angle Wigner functions $D^L_{qq'}(\Omega)$ using far fewer orientations, but no such sets have appeared, to the authors' knowledge. The problem of finding better solutions in the three-angle case is currently under investigation.

SHREWD SCHEMES—OPTIMIZATION OF WEIGHTS

As shown in what follows, the Lebedev schemes appear to be superior to any other method for integration of functions with C_i and D_{2h} symmetry, in the case that $L^f_{\max}$ is less than 53. However, there are some remaining problems with the Lebedev schemes:

1. No Lebedev schemes currently exist for $L_{\max}$ larger than 53.
2. The Lebedev rank profiles often have undesirable behavior beyond $L^S_{\max}$. This leads to nonoptimal performance when only moderate accuracy is required.

For these reasons, we have attempted to combine the ''geometrical'' and ''mathematical'' approaches: The distribution of orientations is based on geometrical arguments, but the weights are provided by optimizing a spherical rank profile. We call these schemes *SHREWD* (Spherical Harmonic Reduction or Elimination by a Weighted Distribution).

The SHREWD strategy will first be stated in its most general form. Consider an arbitrary set of N^S orientations $\Omega_j = (\alpha_j, \beta_j, \gamma_j)$. We wish to integrate exactly a set of target functions $D^L_{qq'}(\Omega)$, where $L = 0, 1, \ldots, L_{\max}$, and the indices q and q' take all possible values. The optimum set of weights $\{w^S_j\}$ may be deduced by solving the linear system of equations

$$\mathbf{M}^S_D \mathbf{w}_S = \sigma_{\text{target}}, \qquad [26]$$

or, in explicit matrix notation,

$$\begin{pmatrix} D^0_{00}(\Omega_1) & D^0_{00}(\Omega_2) & \cdots & D^0_{00}(\Omega_{N^S}) \\ \vdots & \vdots & \ddots & \vdots \\ D^L_{qq'}(\Omega_1) & D^L_{qq'}(\Omega_2) & \cdots & D^L_{qq'}(\Omega_{N^S}) \\ \vdots & \vdots & \vdots & \vdots \end{pmatrix} \begin{pmatrix} w^S_1 \\ w^S_2 \\ \vdots \\ w^S_{N^S} \end{pmatrix} = \begin{pmatrix} 1 \\ 0 \\ \vdots \\ 0 \end{pmatrix}, \qquad [27]$$

where $\mathbf{w}_S$ and σ_{target} are vectors having weights and sampling moments as elements, respectively. Each row in the matrix $\mathbf{M}^S_D$ represent a certain combination of L, q, and q', and the columns correspond to the orientation Ω_j. The last row in the matrix $\mathbf{M}^S_D$ corresponds to $L = q = q' = L_{\max}$.

Since the Wigner functions are complex in general, the number of simultaneous equations N_{eqs} represented in Eq. [27] is almost twice the number of rows in $\mathbf{M}^S_D$.

In principle, solving the linear system allows one to ''destroy'' all Wigner functions out to an arbitrary maximum rank $L_{\max}$. However, the number of angles required to do this is prohibitive in practical cases.

In the following examples, we greatly reduce the dimension of the matrix $\mathbf{M}^S_D$ by taking the special case of two-angle averaging of a real function with C_i and D_{2h} symmetries. In the case of C_i symmetry, one only needs to include rows with L even, $q' = 0$, and $q \geq 0$. This reduces the number of simultaneous equations to

$$N_{\text{eqs}}(C_i) = \frac{1}{2} L_{\max}(L_{\max} + 3) + 1. \qquad [28]$$

For D_{2h} symmetry, the number of equations is reduced further by considering only the real parts of Wigner functions and even q-components:

$$N_{\text{eqs}}(D_{2h}) = \frac{1}{8} (L_{\max} + 4)(L_{\max} + 2). \qquad [29]$$

The columns (rows) of $\mathbf{M}^S_D$ are in general linearly independent. Such a system of linear equations in N^S unknowns conforms to one of three possibilities: (i) The number of unknown weights exactly matches the number of equations: $N^S = \text{N}_{\text{eqs}}$. This provides a set of weights which ensure that all relevant sampling moments exactly vanish for $0 < L \leq L_{\max}$. (ii) The system is *overdetermined*, that is, $N^S < \text{N}_{\text{eqs}}$. We return to this case later. (iii) The system is *underdetermined;* $N^S > \text{N}_{\text{eqs}}$. This case is of no practical interest.

Exact Solutions

We have solved systems of equations using orientations generated by the ZCW algorithm. The solutions with $N_{\text{eqs}} = N^S$ have characteristics similar to those of the Lebedev schemes. However, these sets are approximately three times larger than the Lebedev sets, so these are not of great interest.

The preceding approach may also be applied to the step method. This can be implemented comparatively easily and has the advantage of being *open-ended*, allowing straightforward construction of schemes with arbitrary $L^S_{\max}$. We demonstrate the method over a hemisphere and octant.

These SHREWD-step schemes are constructed as follows: Select an *even* $L_{\max}$ and generate orientations according to

$$\beta_j = \frac{\pi j}{2N_\beta}, \; 1 \leq j \leq N_\beta, \qquad [30]$$

where $N_\beta = \frac{1}{2}L_{\max} + 1$ and

$$\alpha_i = \begin{cases} \dfrac{2\pi i}{N_\alpha},\ 1 \le i \le N_\alpha \text{ for hemisphere} \\ \dfrac{\pi}{4N_\alpha}(2i+1),\ 0 \le i \le N_\alpha - 1 \text{ for octant} \end{cases}, \quad [31]$$

with N_α given by

$$N_\alpha = \begin{cases} L_{\max} + 1 \text{ for hemisphere} \\ \text{ceil}\left\{\dfrac{1}{4}(L_{\max}+1)\right\} \text{ for octant} \end{cases}. \quad [32]$$

The function ceil is defined such that for an argument x, it returns the smallest integer larger than or equal to x.

To each orientation $\{\alpha_i, \beta_j\}$, associate a weight w_j, given as the solution of the following system of equations:

$$\begin{pmatrix} P_0(\cos\beta_1) & P_0(\cos\beta_2) & \cdots & P_0(\cos\beta_{N_\beta}) \\ P_2(\cos\beta_1) & P_2(\cos\beta_2) & \cdots & P_2(\cos\beta_{N_\beta}) \\ \vdots & \vdots & \ddots & \vdots \\ P_{L_{\max}}(\cos\beta_1) & P_{L_{\max}}(\cos\beta_2) & \cdots & P_{L_{\max}}(\cos\beta_{N_\beta}) \end{pmatrix} \begin{pmatrix} w_1 \\ w_2 \\ \vdots \\ w_{N_\beta} \end{pmatrix} = \begin{pmatrix} 1 \\ 0 \\ \vdots \\ 0 \end{pmatrix}, \quad [33]$$

where $P_L(x)$ is the Legendre polynomial of order L. This variant of the step method has weights which are not equal to $\sin\beta_j$, but which are adjusted to provide the accurate quadrature. These schemes are approximately 2.5 times less efficient than the Lebedev schemes. However, the weights are readily calculated out to arbitrarily high ranks, whereas the Lebedev schemes are at present only available up to $L^{\mathrm{S}}_{\max} = 53$. They are therefore of interest when integrating ''difficult'' functions. In the calculations discussed later, we use a SHREWD-STEP scheme with $L^S_{\max} = 100$ to provide highly accurate ''reference'' calculations, with which other methods may be compared. Other schemes have been reported which provide accurate spherical quadrature out to arbitrarily high ranks, while being only 1.5 times less efficient than the Lebedev schemes (*13, 14*).

We have also developed schemes which eliminate increasingly high ranks iteratively, in a purely computational extension of experiments using rotations around multiple axes (*32, 36–38*). So far, this approach has not generated any schemes which are competitive with the Lebedev and SHREWD approaches.

Least-Squares Optimization

We return now to the case when the system in Eq. [27] is overdetermined, so that no exact solution is available. It is still possible to solve for the *least-squares* solution (*31, 39*) to the exact vector σ_{target}. This permits construction of schemes with relatively flat rank-profiles over larger ranges of $L_{\max}$. Best results are obtained by incorporating a function which determines the relative importance given to satisfying each individual equation. For example, it is very important to keep the normalization condition $\sigma^S_{000} = 1$ fulfilled. Furthermore, it is more desirable to keep σ^S_{Lq0} small for low values of L while the values for very large L may be allowed more freedom. This is taken into account by obtaining a *weighted least-squares* (*39*) solution according to

$$\mathbf{G}\mathbf{M}^S_D\mathbf{w}_S = \mathbf{G}\sigma_{\text{target}}, \quad [34]$$

where $\mathbf{G}$ is a diagonal matrix whose elements indicate the relative importance of satisfying each of the simultaneous equations. In practice, the matrix elements of $\mathbf{G}$ are chosen by assuming that the spherical coefficients f_{Lq0} of the function to be integrated decay sharply after $L^f_{\max}$, so that sampling moments σ^S_{Lq0} are less important for $L > L^f_{\max}$. In our evaluations, we assumed a Gaussian curve with respect to L and q, according to

$$\begin{aligned} \mathbf{G}(0,\,0) &= 10^6 \\ \mathbf{G}(L,\,q) &= \exp\{-(L/L_G)^2 - (q/q_G)^2\},\ L > 0, \end{aligned} \quad [35]$$

where L_G and q_G determine the width of the Gaussian function. The large value of $\mathbf{G}(0,\,0)$ ensures that the weights remain almost normalized during the least-squares optimization. Exact normalization of the weights is imposed afterwards.

The weighted least-squares solution of Eq. [34] is given by

$$\mathbf{w}_S = (\mathbf{G}\mathbf{M}^S_D)^+\mathbf{G}\sigma_{\text{target}}, \quad [36]$$

where the cross indicates the pseudo-inverse (*39*).

Best results are obtained by adjusting L_G and q_G according to the number of angles N^S. It is always possible to find weights which perform better than the original ones. We have optimized a number of schemes under different symmetries. We use SHREWD as prefix for the sets with optimized weights. For example, SHREWD-ZCWoct89 is the scheme obtained by refining the weights of the ZCW scheme over an octant using 89 angles. The result of such an optimization is given in Fig. 3. Comparison of the rank-profiles show a markedly improved performance for SHREWD-ZCWoct89 at essentially all ranks up to $\simeq$40. After this value of L, the sampling moments of the two schemes are almost identical. The parameters used in this optimization were $L_G = q_G = 30$, and $L = 30$ was the highest rank included in the system of equations.

The optimization process outlined here is successful for minimizing sampling moments that are already comparatively small. However, large ''peaks'' appearing in the profiles (compare Fig. 2) cannot in general be dealt with. Significant improved performance is only to be expected when the ''peak'' appears at relatively high values of L.

SHREWD weighting cannot perform miracles and transform a poor sampling scheme into a good one. However, it is

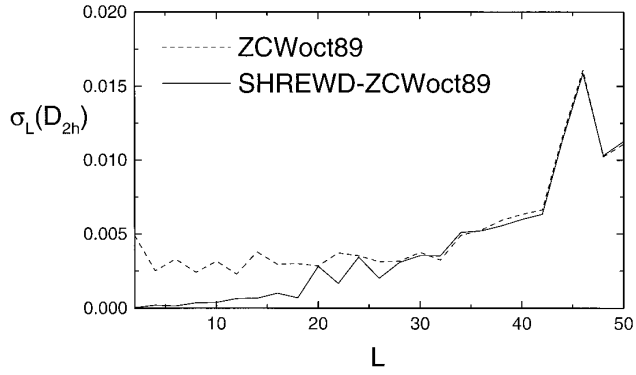

FIG. 3. Rank-profiles for ZCWoct89 and SHREWD-ZCWoct89, where the latter is obtained by least-square optimization of the weights of the former, including $L = 30$ as highest rank in the system of equations and $L_G = q_G = 30$.

capable of improving the performance of a scheme which is already rather good, and gives much faster convergence at a large number of angles. In principle it is also possible to optimize an angle set by allowing the orientations Ω_j^S to vary, while searching for the set of orientations giving the flattest rank-profile. These sets may then be refined further using least-squares optimized weights. This procedure corresponds to a REPULSION-type approach, but with the flatness of the rank profile playing the role of the electrostatic potential.

EVALUATION OF AVERAGING PERFORMANCE

In this section we evaluate the averaging properties of the Lebedev schemes and compare them with some of the most popular geometrical methods. Our test case is the calculation of spinning sideband patterns generated by a single chemical shift anisotropy interaction in MAS NMR. If the principal axis system of the CSA interaction is used, the calculation conforms to D_{2h} symmetry, allowing integration over an octant of the spherical surface. If an arbitrary molecule-fixed axis frame is used, hemispherical schemes appropriate to C_i symmetry are relevant.

Calculation of MAS Sidebands

The calculation of MAS sideband patterns was performed by Herzfeld and Berger (*18*) using truncated Bessel function expansions. The following procedure uses instead a direct time-domain calculation of the form discussed in Ref. (*40*). In order to establish an unambiguous notation, our approach to the problem is now formulated briefly.

Consider a rotating powder containing a set of isolated spin-1/2 sites experiencing a chemical shift anisotropy interaction. The time-dependent Hamiltonian for a certain molecular orientation is

$$H(t, \Omega_{\mathrm{MR}}) = \omega_{\mathrm{CS}}(t, \Omega_{\mathrm{MR}})I_z, \qquad [37]$$

where the periodically modulated chemical shift offset frequency may be written as a Fourier series

$$\omega_{\mathrm{CS}}(t, \Omega_{\mathrm{MR}}) = \sum_{m=-2}^{2} \omega_{\mathrm{CS}}^{(m)}(\Omega_{\mathrm{MR}})\exp\{im\omega_r t\}, \qquad [38]$$

and ω_r is the rotational frequency of the sample. The Fourier components $\omega_{\mathrm{CS}}^{(m)}(\Omega_{\mathrm{MR}})$ are given by

$$\omega_{\mathrm{CS}}^{(m)}(\Omega_{\mathrm{MR}}) = \omega_{\mathrm{iso}}\delta_{m0} + \sum_{m',m''=-2}^{2} [A_{2m''}^{\mathrm{CSA}}]^P D_{m''m'}^2(\Omega_{\mathrm{PM}}) \times D_{m'm}^2(\Omega_{\mathrm{MR}})d_{m0}^2(\beta_{\mathrm{RL}})\exp\{-im\alpha_{\mathrm{RL}}^0 t\}, \qquad [39]$$

where ω_{iso} is the isotropic chemical shift frequency. The angle α_{RL}^0 describes the sample position as $t = 0$ and is immaterial for the present discussion. β_{RL} is the angle between the rotation axis and the field, equal to arctan $\sqrt{2}$ for exact magic angle spinning. The numbers $[A_{2m}^{\mathrm{CSA}}]^{\mathrm{P}}$ are components of the CSA tensor in its principal axis system:

$$[A_{2m}^{\mathrm{CSA}}]^P = \begin{cases} \omega_{\mathrm{aniso}} & \text{if } m = 0 \\ 0 & \text{if } m = \pm 1 \\ -\dfrac{1}{\sqrt{6}}\eta\omega_{\mathrm{aniso}} & \text{if } m = \pm 2 \end{cases}. \qquad [40]$$

The anisotropy ω_{aniso} and asymmetry parameter η characterize the CSA tensor. They are calculated from

$$\omega_{\mathrm{aniso}} = \omega_0(\delta_{zz} - \delta_{\mathrm{iso}}), \qquad [41]$$

$$\eta = \frac{\delta_{yy} - \delta_{xx}}{\delta_{zz} - \delta_{\mathrm{iso}}}, \qquad [42]$$

where $\omega_0 = -\gamma B_0$ is the Larmor frequency of the nucleus and δ_{iso} is the mean of the principal values of the tensor $\delta_{\mathrm{iso}} = (\delta_{xx} + \delta_{yy} + \delta_{zz})/3$. The principal values are expressed in deshielding units and ordered according to $|\delta_{zz} - \delta_{\mathrm{iso}}| \geq |\delta_{xx} - \delta_{\mathrm{iso}}| \geq |\delta_{yy} - \delta_{\mathrm{iso}}|$.

Suppose that the transverse magnetization components are prepared with uniform phase $\phi = 0$ at time $t = 0$. The time-signal generated from the Hamiltonian in Eq. [37] can be expressed as a product of two factors

$$s(t, \Omega_{\mathrm{MR}}) = \exp\{i\omega_{\mathrm{CS}}^{(0)}t\}\exp\{i\Phi_{\mathrm{CS}}(t, 0; \Omega_{\mathrm{MR}})\}. \qquad [43]$$

The periodic phase $\Phi_{\mathrm{CS}}(t, 0; \Omega_{\mathrm{MR}})$ is given by

$$\Phi_{\mathrm{CS}}(t, 0; \Omega_{\mathrm{MR}}) = \int_0^t \omega_{\mathrm{CS}}(\Omega_{\mathrm{MR}}, t')dt' \qquad [44]$$

and can be expressed analytically as

$$\Phi_{\mathrm{CS}}(t, 0; \Omega_{\mathrm{MR}}) = \sum_{m \neq 0} \omega_{\mathrm{CS}}^{(m)}(\Omega_{\mathrm{MR}}) \left\{ \frac{\exp(im\omega_r t) - 1}{im\omega_r} \right\}. \quad [45]$$

The numerical calculation of the MAS spectrum proceeds as follows. The rotational period $\tau_r = 2\pi/\omega_r$ is divided into n segments of equal length $\tau = \tau_r/n$, and the periodic function $\exp\{i\Phi_{\mathrm{CS}}(t, 0; \Omega_{\mathrm{MR}})\}$ is evaluated at each time point $t = p\tau$, with $p = 0, 1, \ldots, n-1$. Discrete Fourier transformation of the set of points gives a manifold of orientation-dependent sideband amplitudes

$$a^{(k)}(\Omega_{\mathrm{MR}}) = n^{-1} \sum_{p=0}^{n-1} \exp\{i[\Phi_{\mathrm{CS}}(t, 0; \Omega_{\mathrm{MR}}) - 2\pi pk/n]\},$$

$$-\frac{n}{2} + 1 \leq k \leq \frac{n}{2}, \quad [46]$$

where k denotes the sideband index.

The number n should be even, and when it is equal to an integer power of 2, a fast Fourier transform (*31*) can be used for optimal computational efficiency. The frequency span of the calculation is given by $n\omega_r$. The number n should be chosen to greatly exceed the number of sidebands in the spectrum. The spectrum consists of a superposition of peaks with amplitudes $a^{(k)}(\Omega_{\mathrm{MR}})$ at frequencies $\omega^{(k)} = \omega_{\mathrm{CS}}^{(0)} + k\omega_r$ (*33, 40*). For exact magic-angle spinning ($\beta_{\mathrm{RL}} = \arctan\sqrt{2}$), the Fourier component $\omega_{\mathrm{CS}}^{(0)}$ is equal to ω_{iso} and the frequencies are orientation-independent. Sidebands for different orientations are exactly superimposed.

The powder averaged sideband amplitude $\bar{a}^{(k)}$ is given by

$$\bar{a}^{(k)} = \langle a^{(k)}(\Omega_{\mathrm{MR}}) \rangle_{\Omega_{\mathrm{MR}}}, \quad [47]$$

where $\langle \cdots \rangle_{\Omega_{\mathrm{MR}}}$ represents an average over Ω_{MR}. As shown in Ref. (*17*), the integration over γ may be taken into account simply by taking the square modulus of the amplitude. The calculation may therefore be reduced to a two-angle integral:

$$\bar{a}^{(k)} = \int_{V^{(2)}} |a^{(k)}(\alpha_{\mathrm{MR}}, \beta_{\mathrm{MR}}, 0)|^2 d\Omega. \quad [48]$$

The squared sideband amplitudes are the target functions for orientational averaging: $f^{(k)}(\Omega) = |a^{(k)}(\Omega_{\mathrm{MR}})|^2$. Integration is performed by a weighted summation over sets of $(\alpha_{\mathrm{MR}}, \beta_{\mathrm{MR}})$ pairs, as described earlier.

We have verified that the spread of $L_{\max}$ among the various sideband orders is rather uniform in typical cases. The rms rank-profiles $f_L^{(k)} = |a^{(k)}|_L^2$ for a set of sideband indices k are plotted against L in Fig. 4.

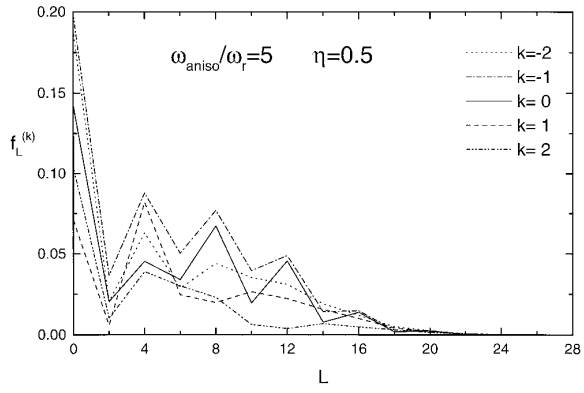

FIG. 4. (a) Rank profiles of MAS sideband functions $f_L^{(k)}$, $-2 \leq k \leq 2$, for the case of a CSA tensor with $\eta = 0.5$ and $\omega_{\mathrm{aniso}}/\omega_r = 5$. The estimated $L_{\max}$ is approximately the same for all sidebands. Accurate orientational averaging requires schemes with small sampling moments below rank ≃22. Because of D_{2h} symmetry, the odd rank components are all zero and are not shown.

Calculations in the Principal Axis System

Calculation of MAS spinning sideband patterns is performed most efficiently by choosing the molecular reference frame M to coincide with the principal axis system P of the CSA interaction. This implies using $\Omega_{\mathrm{PM}} = (0, 0, 0)$ in Eq. [39]. The γ-averaged sideband amplitudes $|a^{(k)}(\alpha_{\mathrm{MR}}, \beta_{\mathrm{MR}})|^2$ possess D_{2h} symmetry with respect to the angles $(\alpha_{\mathrm{MR}}, \beta_{\mathrm{MR}})$, allowing the use of greatly reduced Lebedev schemes.

We have evaluated different averaging schemes by first calculating a ''reference'' sideband pattern, using a SHREWD-STEPoct scheme with $L_{\max}^S = 100$ requiring 1326 orientations. This calculation gave essentially identical results to a conventional step method calculation using 10^6 orientations. In all cases, n was chosen to be much larger than the number of significant sidebands, and it was verified that further increase in n did not significantly affect the sideband amplitudes. The reference spectrum may therefore be considered to be exact.

The powder performance of each scheme was evaluated by calculating the maximum deviation in sideband amplitudes $\bar{a}_S^{(k)}$, relative to the reference spectrum $\bar{a}_{\mathrm{ref}}^{(k)}$ over the entire set of sidebands:

$$\epsilon_{\max}^S = \max_k\{|\bar{a}_S^{(k)} - \bar{a}_{\mathrm{ref}}^{(k)}|\}, \; -\frac{n}{2} + 1 \leq k \leq \frac{n}{2}, \quad [49]$$

where $\bar{a}_S^{(k)}$ is the integrated sideband amplitude when using scheme S. Since the largest sidebands in the spectrum tend to have the largest errors, this error function has the advantage of being independent of the number of evaluated sidebands, as long as the calculation has sufficient bandwidth n. Other evaluation criteria have also been tried. The conclusions reached about relative integration properties for different schemes are essentially independent of the choice of evaluation method, as long as systematic errors are avoided.

Plots of $\epsilon_{\max}^S$ are shown in Fig. 5 for different shift anisotro-

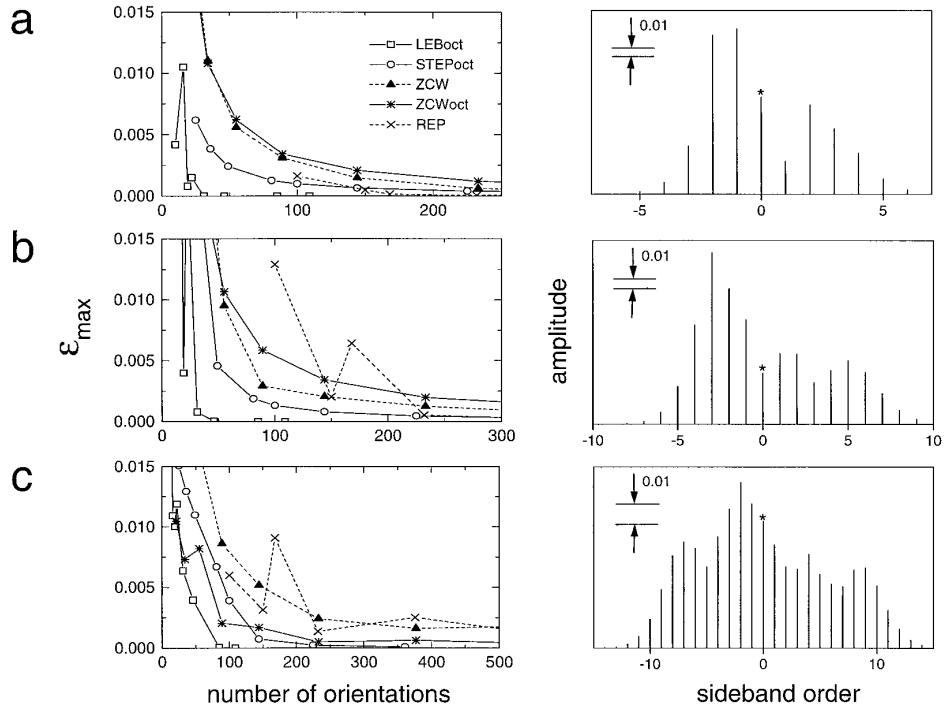

FIG. 5. Powder averaging performance for MAS sideband amplitudes from a CSA tensor in its principal axis system. Five powder approaches were used: ZCW and REPULSION over full sphere, denoted ZCW and REP, respectively, and octant versions of ZCW (ZCWoct), Lebedev (LEBoct), and step method (STEPoct). Left diagrams: Maximum sideband error $\epsilon_{\max}$ (Eq. [49]) for each scheme plotted against number of orientations. Right diagrams: MAS spectrum (amplitudes). (a) $\omega_{\text{aniso}}/\omega_r = 5$ and $\eta = 0.3$. (b) $\omega_{\text{aniso}}/\omega_r = 8$ and $\eta = 0.3$. (c) $\omega_{\text{aniso}}/\omega_r = 12$ and $\eta = 0.7$.

pies and asymmetry parameters. The following schemes are evaluated: Lebedev over octant (LEBoct), REPULSION (REP), ZCW over full sphere (ZCW) and octant (ZCWoct), and step-method over octant (STEPoct). In Fig. 5a, the case $\omega_{\text{aniso}}/\omega_r = 5$ and $\eta = 0.3$ is investigated. The Lebedev method converges very rapidly and reduces the error below 0.0025 using a scheme with $L^S_{\max} = 17$, requiring only 19 angles. The error is reduced to $\epsilon^S_{\max} \simeq 10^{-5}$ using only 31 orientations, corresponding to a scheme with $L^S_{\max} = 23$. None of the other schemes reach this accuracy with fewer than 1000 orientations. In this regime of shift anisotropy, the REPULSION method outperforms ZCW. Orientational averaging using randomly chosen points on the sphere requires around 20,000 orientations to reduce the error to below ~0.0025. The computational speeds for the best (Lebedev) and worst (random) methods differ by a factor of 1000.

The Lebedev schemes also outperform the other approaches in the more demanding case in Fig. 5b, in which the ratio $\omega_{\text{aniso}}/\omega_r$ is increased to 8, keeping the asymmetry parameter constant at $\eta = 0.3$. A markedly decreased performance is noted for the REPULSION schemes, which is even more pronounced in Fig. 5c, where the following CSA parameters are used: $\omega_{\text{aniso}}/\omega_r = 12$ and $\eta = 0.7$. It should be noted, however, that the REPULSION sets are not adapted to the symmetry of the function.

In all three cases depicted in Fig. 5, the Lebedev octant sets are clearly the best choice for integration. The Lebedev sets only experience significant competition in more demanding cases such as in Fig. 5c, where the ZCWoct and STEPoct schemes start to gain ground slightly.

The case in Fig. 5b is examined more closely in Fig. 6. Here the computed sideband amplitudes for different schemes are compared with an exact reference spectrum. In Figs. 6a, d, and g, all schemes involve around 20 angles. None of these have converged. LEBoct31 is compared with ZCWoct34 and STEPoct36 in Figs. 6b, e, and h. There is almost no visual difference between the spectra obtained from the Lebedev set and the reference spectrum. All of the other powder methods show strong deviations. In Figs. 6c, f, and i, these schemes are compared for around 85 angles. The STEPoct scheme has now attained near-convergence, while the ZCWoct method still shows deviations.

The comparison in Fig. 5 also reveals an interesting distinction between ZCW schemes in which sampling points are distributed over a full sphere, and those in which the points are restricted to an octant. Generally speaking, we have found the octant version to be better in cases with $\eta > 0.5$, while the full sphere version is often better for $\eta < 0.5$, and is *always* superior when a very large number of orientations ($N^S > 400$) is used to obtain high accuracy.

It is perhaps surprising that ZCWoct is not always superior to ZCW, given that the density of sampling points is much higher in the octant case. It seems that the accuracy of numerical integration depends on subtle details of the sampling and

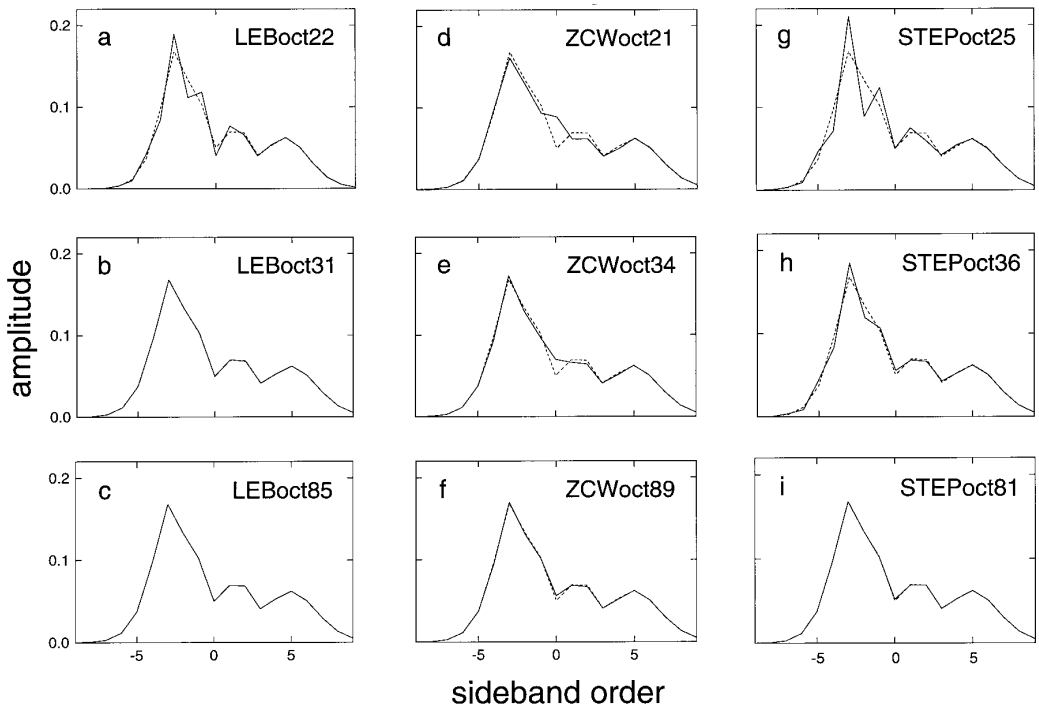

FIG. 6. Calculated MAS sideband amplitudes for some of the schemes used in Fig. 5b, compared with an exact reference spectrum (ref). For clarity, the sideband amplitudes are joined by continuous lines (for the evaluated scheme) and dotted lines (for the exact spectrum). (a) Lebedev over octant with (a) 22, (b) 31, and (c) 85 orientations; ZCW over octant for (d) 21, (e) 34, and (f) 89 orientations; and STEPoct with (g) 25, (h) 36, and (i) 81 orientations.

cannot be quantified by a simple criterion such as sampling point density. The poor performance of octant versions of ZCW at large number N^S may be related to the fact that ZCW was originally developed for integration over rectangular bounds in two dimensions. The boundary conditions in octant integration on the surface of a sphere are quite different.

The improvement of performance of ZCWoct and REPULSION through SHREWD weighting is illustrated in Fig. 7. The simulation parameters of Fig. 5a were used (note the magnified scale). The superiority of SHREWD-ZCWoct over ZCWoct is obvious. Different versions of REPULSION are also contrasted: REP uses weights as described in Ref. (*25*). The schemes SHREWD-REP were obtained from an least-squares optimization, as described earlier. Although SHREWD weighting provides some improvement, all of these methods are still clearly outperformed by the Lebedev schemes. Presumably, the performance of REPULSION would be further enhanced by adapting it to the symmetry of the function, as suggested in Ref. (*25*).

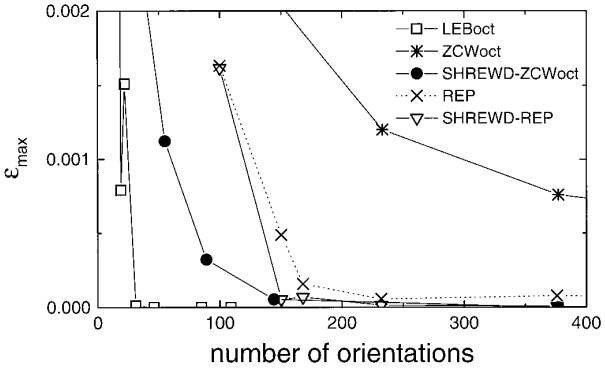

FIG. 7. Demonstration of improved powder schemes by optimization of the weights for REPULSION and ZCWoct. The parameters are same as in Fig. 5a, but the scale is enlarged. The schemes are REPULSION with weights as described in Ref. (*25*), REPULSION with least-squares optimized weights (SHREWD-REP), and ZCWoct with least-squares optimized weights (SHREWD-ZCWoct). The performance of the Lebedev octant schemes is also shown.

Calculations in an Arbitrary Molecular Frame

It is also possible to calculate MAS sideband amplitudes using an arbitrary molecular frame *M*, instead of the principal axis frame *P*. The calculation then involves an extra $P \rightarrow M$ transformation, as described in Eq. [39]. The orientational variable in this case is $\Omega_{MR} = (\alpha_{MR}, \beta_{MR}, \gamma_{MR})$.

For an isolated spin-1/2 site, there is no advantage in using an arbitrary frame *M* instead of the principal axis frame *P*. The calculation is introduced here merely as an example with C_i symmetry of the orientational function.

The γ-averaged sideband amplitudes $|a^{(k)}(\alpha_{MR}, \beta_{MR})|^2$ have the symmetry property (*17, 41*)

$$|a^{(k)}(\alpha_{MR}, \beta_{MR}, 0)|^2 = |a^{(k)}(\alpha_{MR} + \pi, \pi - \beta_{MR}, 0)|^2. \quad [50]$$

This allows the integration to be performed over only one

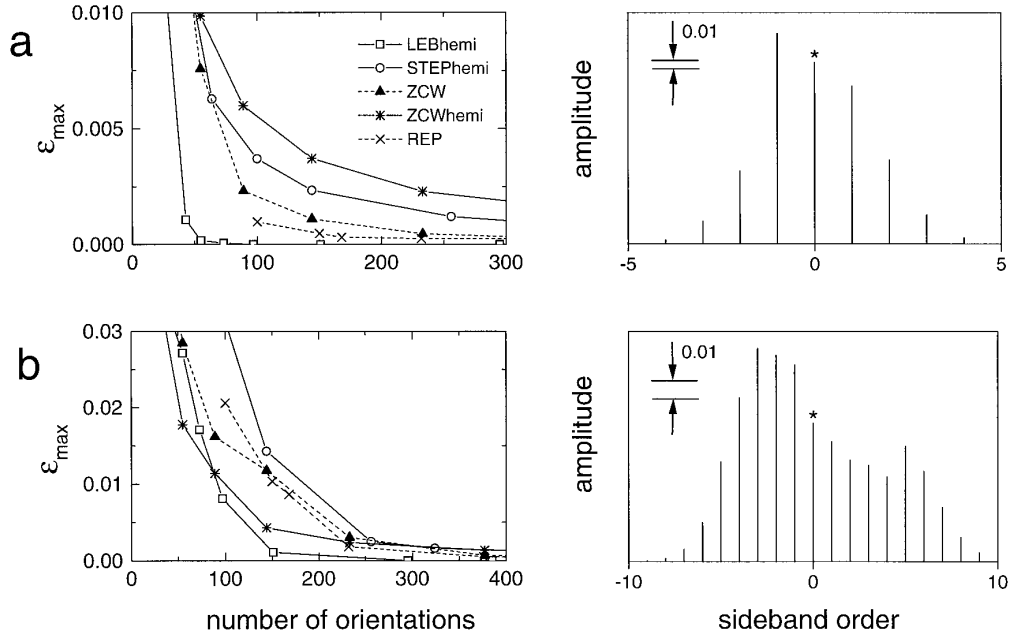

FIG. 8. Powder averaging performance for MAS sideband amplitudes using a CSA tensor in a set of 100 arbitrary molecular reference frames. Five powder approaches were used: ZCW and REPULSION over full sphere (ZCW) and (REP), respectively, and hemispheric versions of ZCW (ZCWhemi), Lebedev schemes (LEBhemi), and step method (STEPhemi). Left diagrams: Maximum sideband errors ϵ_{max} (Eq. [52]) for each scheme plotted against number of orientations. Right diagrams: MAS spectrum (amplitudes). (a) $\omega_{aniso}/\omega_r = 3$ and $\eta = 0.8$. (b) $\omega_{aniso}/\omega_r = 8$ and $\eta = 0.5$.

hemisphere $0 \le \alpha_{MR} < 2\pi$, $0 \le \beta_{MR} \le \pi/2$. Integration may be performed using ''hemispheric'' Lebedev sets which have exactly half the number of angles of the full Lebedev sets.

Consider a calculation of the powder averaged sideband amplitude $\bar{a}^{(k)}$ using a certain sampling scheme for orientations Ω_{MR}. In general the result of this calculation depends on the relative orientation Ω_{PM} of the principal axis frame and the molecular reference frame, and may therefore be denoted

$$\bar{a}_S^{(k)}(\Omega_{PM}) = \sum_j w_j^S |a^{(k)}(\Omega_{PM}, \Omega_{MR}^j)|^2. \qquad [51]$$

To avoid systematic bias due to a particular choice of transformation Ω_{PM}, we follow Bak and Nielsen (*25*) and repeat the calculation for a large number of transformations Ω_{PM}. In practice, we used 100 randomly chosen orientations. The error criterion used for evaluation of the schemes was

$$\epsilon_{max}^S = \max\{|\bar{a}_S^{(k)}(\Omega_{PM}^l) - \bar{a}_{ref}^{(k)}|\}_{k,l},$$
$$-\frac{n}{2} + 1 \le k \le \frac{n}{2},\ 1 \le l \le 100, \qquad [52]$$

that is, the largest absolute error in any spinning sideband amplitude, scanned over all choices of reference frame *M*. The reference amplitudes $\bar{a}_{ref}^{(k)}$ were obtained from converged calculations using the principal axis frame. The criterion ϵ_{max}^S is roughly independent of the number of sidebands involved in the calculation and also of the ensemble of molecular frames *M*, once a sufficient number is chosen.

The Lebedev sets again give fastest convergence. In Fig. 8a the CSA parameters are $\omega_{aniso}/\omega_r = 3$ and $\eta = 0.8$. All methods converge to approximately 1% accuracy within 100 angles. However, the Lebedev sets converge faster than any other scheme. The next best in this regime is REPULSION.

In Fig. 8b a more difficult case is investigated: $\omega_{aniso}/\omega_r = 8$ and $\eta = 0.5$. Again, the Lebedev sets converge faster than any other method, although the ZCW hemispheric sets now offers significant competition. The ZCW and REPULSION full-sphere sets have very similar behavior.

PRACTICAL RECOMMENDATIONS

The subject of orientational averaging in solid-state NMR is very complex. The best strategy to use depends on (i) the symmetry of the NMR response with respect to orientation, and (ii) whether only the *amplitudes* of the peaks are orientation-dependent, or both the amplitudes and the peak *frequencies* are orientation-dependent.

Orientation-Dependent Peak Amplitudes Only

At the moment, Gaussian spherical quadratures appear to be most useful for cases where the peak amplitudes are orientation-dependent, but the peak frequencies are not. This includes many dynamically inhomogeneous problems, such as the spectrum generated by isolated spins-1/2 under exact magic-angle

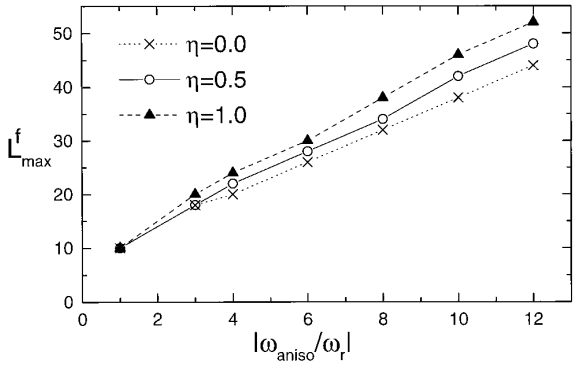

FIG. 9. Estimated $L^f_{\max}$ for different ratios $\omega_{\text{aniso}}/\omega_r$ and asymmetry parameters η.

spinning, as evaluated earlier. Another example is the evolution of multiple-quantum coherences under heteronuclear local fields, as in the recently developed experiments for determining molecular torsional angles (*4–7*).

For such applications, it is useful to have some insight into the maximum spherical rank $L^f_{\max}$ of the function to be averaged. We have evaluated rank profiles for a variety of asymmetry parameters η and ratios in the range $1 \leq |\omega_{\text{aniso}}/\omega_r| \leq 12$ for the case of exact magic-angle-spinning of isolated spins-1/2. In Fig. 9, plots of $L^f_{\max}$ against the ration $|\omega_{\text{aniso}}/\omega_r|$ for three different asymmetry parameters are shown. $L^f_{\max}$ grows as both $|\omega_{\text{aniso}}/\omega_r|$ and η increase. For a fixed η, $L^f_{\max}$ depends almost linearly on $|\omega_{\text{aniso}}/\omega_r|$.

As discussed in Ref. (*42*), ω_{aniso} is usually most reliably determined from experiments using $3 \lesssim |\omega_{\text{aniso}}/\omega_r| \lesssim 5$. By comparing with Table 1, we see that in this range, calculations using LEBoct schemes requires *at most* 31 orientations for highly accurate sideband amplitudes (assuming D_{2h} symmetry). On the other hand, for rotating solids, the most reliable determinations of the asymmetry parameter are generally made in the slow-spinning region of $|\omega_{\text{aniso}}/\omega_r| \gtrsim 10$ (*42*). This is in general outside the range of applicability of the Lebedev schemes, and here SHREWD schemes may be used instead.

Figure 9 may also be used in more general situations, as long as only the peak amplitudes depend on orientation, and not the peak frequencies. The value of $L^f_{\max}$ may be estimated by replacing ω_{aniso} with ω_{int}, the size of the interaction under study. If several interactions are involved, a very conservative estimate of $L^f_{\max}$ is obtained by using the sum of all $|\omega_{\text{int}}|$. In many cases, the convergence is much faster than predicted, especially if the calculation is made in the PAS.

For problems of this type, the function to be averaged always display orientational symmetry, so the reduced hemispherical or octant Lebedev sets should be used, as appropriate.

Orientation-Dependent Peak Amplitudes and Frequencies

In most computationally intensive problems, both the peak amplitudes and peak frequencies $\omega^{(k)}$ are orientation-dependent. Our limited experience with these more general cases suggests that the rank profiles of the amplitudes $a^{(k)}$ and sideband frequencies $\omega^{(k)}$ both cut off at about the same rank as indicated in Fig. 9, if the sum of sizes of all interactions ω_{int} is used. However, in general, the rank profile of the total *spectrum* $S(\omega)$ often displays a much slower convergence. This is because the amplitude of a certain point in the *spectrum* may be a very sharp function in orientational space, even when the frequency of the resonance *peaks* has a smooth orientation dependence. As a result, the maximum rank required in the Lebedev schemes is usually much larger than expected from Fig. 9. In these cases, it seems that the Lebedev schemes cannot reduce the number of orientations required for lineshape simulations. Preliminary tests indicate that the Lebedev schemes give similar performance to the ZCW and REPULSION methods for a comparable number of angles, while in some cases, the Lebedev sets are worse. The Lebedev schemes do, however, perform best if the required frequency resolution is low, or equivalently, at relatively short times in time-domain simulations.

It is probably feasible to develop computational algorithms which calculate the spectrum $S(\omega)$ through an estimation of the accurate orientation dependence of the frequencies $\omega^{(k)}$ and $a^{(k)}$, rather than by a crude accumulation of amplitudes at a set of spectral frequency coordinates. By using Lebedev sampling of the calculated peak frequencies, in conjunction with a library of precomputed Wigner functions at the Lebedev angles, it should be possible to estimate very accurately all the spherical moments $f_{Lqq'}$ of both the peak amplitudes and the peak frequencies. The full orientation dependence of the NMR response is therefore defined precisely using a minimal number of computed orientations. Conversion of this information into the spectrum is nontrivial, but it should be possible to exploit interpolation algorithms (*20, 22–24, 30*). This is an interesting direction for future research.

CONCLUSIONS

Gaussian spherical quadrature is used in many fields outside of NMR to obtain accurate spherical integrals with minimal computational effort. The main conclusion of this article is that these schemes can also offer significant advantages for the calculation of certain types of powder average in solid-state NMR. The Lebedev sets are particularly well adapted to problems in which the amplitudes of the NMR peaks are orientation-dependent, while the peak frequencies are not. The Lebedev sets are probably close to the global optimum in these cases and can save large factors of computational time.

In this paper we have also demonstrated that any other sampling scheme may be improved by optimizing the weights to minimize a selected set of spherical sampling moments.

Gaussian spherical quadrature has an advantage over other methods only if the spherical components of the averaged function become very small beyond a maximum spherical rank $L^f_{\max}$. For the NMR spectrum, this usually

holds only if the peak amplitudes, but not the peak frequencies, depend on orientation. We do, however, anticipate the development of new algorithms which exploit the power of the Gaussian spherical quadrature methods even in very general cases.

In this article, we have also classified solid-state NMR problems in terms of the orientational symmetry they display and showed how this symmetry may be used to speed up the numerical computation. Certain orientational sampling schemes, such as the Lebedev sets, are well adapted to symmetry reduction. In other cases, for example the ZCW angle sets, restriction to a fraction of the orientational space does not appear to produce such large improvements.

In summary, the Lebedev sets do not represent a completely general solution for the optimal calculation of powder averages in solid-state NMR, but do offer very significant gains for certain classes of problems. For the calculation of MAS spinning sideband patterns, the use of Lebedev sets can reduce the required computational time by large factors.

All orientational sampling schemes used in this article may be obtained from the authors upon request or directly from the Web site http://www.fos.su.se/physical/mhl/home.html.

APPENDIX 1

Specification of Orientational Averaging Schemes

The performance of orientational averaging schemes is very sensitive to small details, and a number of minor variants exist in the literature. We specify here the methods which we used in our evaluations.

Step Method

The implementation of the STEP method listed here appears to be more efficient than other versions we have tested.

We assume the ranges of integration for the α and β angles to be divided into N_α and N_β segments, respectively, giving a total number of orientations $N_{\text{step}} = N_\alpha N_\beta$. In the calculations in this paper, we use equal steps in the angles α and β, giving $N_\alpha = 4N_\beta$ for the hemisphere and $N_\alpha = N_\beta$ for the octant.

For the *hemisphere* we integrate over $\{0 \le \alpha < 2\pi, 0 \le \beta \le \pi/2\}$, selecting angles as follows:

$$\alpha_i = \frac{2\pi}{N_\alpha} i,\ 0 \le i \le N_\alpha - 1, \qquad [53]$$

$$\beta_j = \frac{\pi}{4N_\beta}(2j+1), 0 \le j \le N_\beta - 1. \qquad [54]$$

This gives a set $S_{\text{hemi}} = \{w_j^S, \alpha_i^S, \beta_j^S\}$ with weights depending on only the β angle, according to

$$w_j^S = \mathcal{N}_{\text{step}} \sin\beta_j, \qquad [55]$$

where $\mathcal{N}_{\text{step}} = (N_\alpha \sum_{j=0}^{N_\beta - 1} \sin\beta_j)^{-1}$.

Integrating over an *octant* corresponds to the ranges $\{0 \le \alpha \le \pi/2, 0 \le \beta \le \pi/2\}$, using the angles

$$\alpha_i = \frac{\pi}{4N_\alpha}(2i+1),\ 0 \le i \le N_\alpha - 1 \qquad [56]$$

$$\beta_j = \frac{\pi}{4N_\beta}(2j+1),\ 0 \le j \le N_\beta - 1, \qquad [57]$$

and weights as in Eq. [55].

ZCW

The sets from the ZCW algorithm are generated from numbers g_M, where M is an integer. These are given recursively from

$$g_M = g_{M-2} + g_{M-1},\ M = 0, 1, 2, \ldots, \qquad [58]$$

with $g_0 = 8$ and $g_1 = 13$. For a given M, the set contains

$$N_M = g_{M+2} \qquad [59]$$

orientations, comprising the following angles:

$$\alpha_j^M = \frac{2\pi}{c_3} \text{mod}\{jg_M/N_M, 1\}, 0 \le j \le N_M - 1 \qquad [60]$$

$$\beta_j^M = \arccos[c_1(c_2 \text{mod}\{j/N_M, 1\} - 1)], 0 \le j \le N_M - 1. \qquad [61]$$

Here c_1, c_2, and c_3 are components of a vector $\mathbf{c}$, which depends on the range of integration. We have for

(a) full sphere: $\mathbf{c} = (1, 2, 1)$
(b) Hemisphere: $\mathbf{c} = (-1, 1, 1)$
(c) Octant: $\mathbf{c} = (-1, 1, 4)$

In the ZCW schemes, the weights are equal, $w_j^M = N_M^{-1}$.

APPENDIX 2

Orientational Symmetry in Solid-State NMR

In this appendix, we explore the orientational symmetry of solid-state NMR signals. Although some of these symmetries are obvious, some only appear after ''carousel averaging'' over one of the orientational angles (*17*).

Consider the general case of the NMR signal $s(t, \Omega_{\text{MR}})$ generated by a nuclear spin system at time t from molecules with orientation Ω_{MR}, specified as the three Euler angles (α_{MR}, β_{MR}, γ_{MR}), relating a molecule-fixed frame M to a frame R fixed with respect to a sample holder. In general, the sample holder may itself be rotating, so the Euler angles $\Omega_{\text{RL}} = (\alpha_{\text{RL}}, \beta_{\text{RL}}, \gamma_{\text{RL}})$ relating the frame R to a fixed ''laboratory'' frame L are time-dependent. For rotation at a fixed angular frequency ω_r about the z-axis of frame R, the first Euler angle is $\alpha_{\text{RL}} =$

$\alpha^0_{\mathrm{RL}} - \omega_r t$, while β_{RL} is the angle subtended by the z-axis of frames R and L. It is usual to define the z-axis of frame L as the field direction so that β_{RL} is the angle subtended by the spinning axis and the field. The angle α^0_{RL} defines the orientation of the frame R at time $t = 0$, which is defined here as the start of the NMR signal acquisition. For simplicity, the frame R is chosen such that $\alpha^0_{\mathrm{RL}} = 0$ in the following discussion. In high-field NMR the angle γ_{RL} does not affect any observations and may be chosen arbitrarily.

The high-field truncated Hamiltonian at time t for molecules in orientation Ω_{MR} may be written

$$H(t, \Omega_{\mathrm{MR}}) = \sum_{\Lambda} H_{\Lambda}(t, \Omega_{\mathrm{MR}}), \qquad [62]$$

with

$$H_{\Lambda}(t, \Omega_{\mathrm{MR}}) = [A^{\Lambda}_{L0}]^L T^{\Lambda}_{\lambda 0}, \qquad [63]$$

where the sum is over spin interactions Λ, and $T^{\Lambda}_{\lambda\mu}$ is the μth component of an irreducible spherical spin operator of rank λ. Similarly, $[A^{\Lambda}_{LM}]^F$ is the mth component of an irreducible spherical tensor of rank L, expressed in frame F. Such tensors may be transformed between the general frames F and G, using Wigner functions:

$$[A^{\Lambda}_{Lm}]^F = \sum_{m'} [A^{\Lambda}_{Lm'}]^G D^L_{m'm}(\Omega_{GF}). \qquad [64]$$

In general, the ''spatial rank'' L is not necessarily equal to the ''spin rank'' μ, because some spin interactions involve a three-way interplay of spins, molecular properties, and the external field. In much literature the ''spin part'' of an interaction is actually a conflation of spin terms and the external magnetic field, a practice which is best avoided because it obscures the rotational symmetry of the interactions with respect to the spin polarizations alone. In the present discussion, λ refers to the irreducible spherical rank with respect to rotations of the spin polarizations (keeping the molecules and external fields fixed), and L refers to the irreducible spherical rank with respect to rotations of the molecules (keeping the spin polarizations and external fields fixed). For example, some common spin interactions have the following spin/space ranks: Isotropic chemical shift: $\lambda = 1$; $L = 0$. Chemical shift anisotropy: $\lambda = 1$; $L = 2$. Antisymmetric chemical shift: $\lambda = 1$; $L = 1$. Scalar spin–spin coupling: $\lambda = 0$; $L = 0$. J-coupling anisotropy: $\lambda = 2$; $L = 2$. Through-space spin–spin coupling: $\lambda = 2$; $L = 2$. Antisymmetric J-coupling: $\lambda = 1$; $L = 1$.

Most of the $L = 1$ terms do not appear in the high-field truncated spin Hamiltonian. The only exception is the antisymmetric J-coupling term ($\lambda = 1$; $L = 1$), which has, however, never been observed in practice.

In a rotating sample, each interaction Λ is periodically modulated, so that

$$H_{\Lambda}(t, \Omega_{\mathrm{MR}}) = \sum_m H^{(m)}_{\Lambda}(\Omega_{\mathrm{MR}}) \exp\{im\omega_r t\}, \qquad [65]$$

and

$$H^{(m)}_{\Lambda}(\Omega_{\mathrm{MR}}) = [A^{\Lambda}_{Lm}]^R d^L_{m0}(\beta_{\mathrm{RL}}) T^{\Lambda}_{\lambda 0}, \qquad [66]$$

where the rotor-frame spherical tensor is

$$[A^{\Lambda}_{Lm}]^R = \sum_{m'} [A^{\Lambda}_{Lm'}]^M D^L_{m'm}(\Omega_{\mathrm{MR}}). \qquad [67]$$

The NMR signal from an orientation Ω_{MR} at time t is given by

$$s(t, \Omega_{\mathrm{MR}}) = \mathrm{Tr}\{Q^{\dagger}_{\mathrm{obs}} \hat{V}(t, 0; \Omega_{\mathrm{MR}}) \rho(0, \Omega_{\mathrm{MR}})\}, \qquad [68]$$

where Q_{obs} is the observable spin operator and $\rho(0)$ is the spin density operator at the beginning of observation. $\hat{V}$ is the propagation superoperator, satisfying the equation

$$\frac{d}{dt} \hat{V}(t, t_a; \Omega_{\mathrm{MR}}) = -i\hat{H}(t, \Omega_{\mathrm{MR}}) + \hat{\Gamma}(t, \Omega_{\mathrm{MR}})$$
$$\hat{V}(t_a, t_a; \Omega_{\mathrm{MR}}) = \hat{1}, \qquad [69]$$

where $\hat{H}$ is the Hamiltonian commutation superoperator and $\hat{\Gamma}$ is the relaxation superoperator. In this appendix, we explore the symmetry of $s(t, \Omega_{\mathrm{MR}})$ with respect to orientation Ω_{MR}.

In the general case, there appears to be no symmetry of $s(t, \Omega_{\mathrm{MR}})$ in the three-dimensional orientational space of (α_{MR}, β_{MR}, γ_{MR}). However, it is worth mentioning an interesting symmetry property with respect to *reversal* of the *sense of rotation* of the sample. The following symmetries of the Wigner functions (*16*),

$$D^L_{mm'}(\pi + \alpha_{\mathrm{MR}}, \pi - \beta_{\mathrm{MR}}, \pi - \gamma_{\mathrm{MR}}) = (-1)^{L+2m+m'} D^L_{m-m'}(\alpha_{\mathrm{MR}}, \beta_{\mathrm{MR}}, \gamma_{\mathrm{MR}}) \qquad [70]$$

$$d^L_{m0}(\beta_{\mathrm{MR}}) = (-1)^m d^L_{-m0}(\beta_{\mathrm{MR}}), \qquad [71]$$

may be used to demonstrate the property

$$H^{(m)}_{\Lambda}(\Omega_{\mathrm{MR}}) = (-1)^L H^{(-m)}_{\Lambda}(\bar{\Omega}_{\mathrm{MR}}), \qquad [72]$$

where the orientation $\bar{\Omega}_{\mathrm{MR}}$ is related to $\Omega_{\mathrm{MR}} = (\alpha_{\mathrm{MR}}, \beta_{\mathrm{MR}}, \gamma_{\mathrm{MR}})$ as follows:

$$\bar{\alpha}_{\mathrm{MR}} = \pi + \alpha_{\mathrm{MR}}$$
$$\bar{\beta}_{\mathrm{MR}} = \pi - \beta_{\mathrm{MR}}$$
$$\bar{\gamma}_{\mathrm{MR}} = \pi - \gamma_{\mathrm{MR}}. \qquad [73]$$

The spin Hamiltonians at a given time t, for the orientations Ω_{MR} and $\bar{\Omega}_{\mathrm{MR}}$ and rotation frequency ω_r, are therefore related through

$$H_\Lambda(t, \omega_r, \Omega_{\mathrm{MR}}) = (-1)^L H_\Lambda(t, -\omega_r, \bar{\Omega}_{\mathrm{MR}}). \qquad [74]$$

Now in a *powder sample*, all orientations Ω_{MR} are equally represented. If all spatial ranks L are *even*, it follows that the NMR signal from a powder sample is independent of the *sign* of ω_r, that is, the sense of rotation. If an orientation Ω_{MR} experiences a certain sequence of spin Hamiltonians when rotating the sample in one direction, then a different orientation $\bar{\Omega}_{\mathrm{MR}}$ experiences precisely the same sequence of spin Hamiltonians when rotating the sample in the opposite direction. In a finely divided powder, the total NMR signal is independent of the sense of rotation. The same conclusions were reached in a different way by Gullion and Conradi (*19*).

Interestingly, this conclusion is strictly valid only if all spin interactions have *even* spatial ranks L. Odd-spatial-rank interactions (such as the antisymmetric J-coupling) might therefore be detected by comparing signals from finely divided powder samples rotating in opposite senses.

We now examine the consequence of *dynamical inhomogeneity* (*33*) of the spin Hamiltonian $H(t)$, that is the case where the Hamiltonian commutes with itself at different times, so its eigenstates may be chosen to be time-independent. The eigenvalues of $H(t, \Omega)$ are denoted $\omega_u(t, \Omega)$ and are periodically modulated:

$$\omega_u(t, \Omega) = \sum_m \omega_u^{(m)}(\Omega)\exp\{im\omega_r t\}, \qquad [75]$$

where the eigenvalue Fourier components are $\omega_u^{(m)}(\Omega)$. In this and subsequent equations, Ω_{MR} is written Ω for simplicity. The NMR signal for dynamically inhomogeneous evolution may be expressed

$$s(t, \Omega) = \sum_{uv} s_{uv}(t, \Omega). \qquad [76]$$

where s_{uv} is the signal associated with coherence $|u\rangle\langle v|$, given by

$$s_{uv}(t, \Omega) = Z_{uv}\exp\{i\Phi_{uv}(t, 0; \Omega)\}. \qquad [77]$$

Here Z_{uv} is the amplitude for excitation and detection of coherence $|u\rangle\langle v|$:

$$Z_{uv} = \langle u|Q_{\mathrm{obs}}^{\dagger}|v\rangle\langle v|\rho(0)|u\rangle. \qquad [78]$$

It is an important feature of the following discussion that $\rho(0)$ and hence Z_{uv} are assumed to be independent of Ω. This is in general only true for simple pulse sequences such as idealized single-pulse excitation or idealized Hartmann–Hahn cross-polarization.

The angle $\Phi_{uv}(t_b, t_a; \Omega)$ is the accumulated dynamic phase of the coherence $|u\rangle\langle v|$ over the interval $t_a \rightarrow t_b$, given by

$$\Phi_{uv}(t_b, t_a; \Omega) = -\int_{t_a}^{t_b} \omega_{uv}(t, \Omega)dt, \qquad [79]$$

where $\omega_{uv}(t, \Omega) = \omega_u(t, \Omega) - \omega_v(t, \Omega)$. This phase angle may be written in general

$$\Phi_{uv}(t_b, t_a; \Omega) = \exp\{-\mathrm{i}(t_b - t_a)\bar{\omega}_{uv}(\Omega)\}\exp\{i\xi_{uv}(t_b, \Omega)\} \times \exp\{-i\xi_{uv}(t_a, \Omega)\},$$

where $\bar{\omega}_{uv}(\Omega)$ is the difference in the average of eigenvalues $\bar{\omega}_u(\Omega) - \bar{\omega}_v(\Omega)$ over the rotor period, and the ξ-functions are defined (*43*)

$$\xi_{uv}(t, \Omega) = -\sum_{m\neq 0} \frac{\{\omega_u^{(m)}(\Omega) - \omega_v^{(m)}(\Omega)\}\exp\{im\omega_r t\}}{im\omega_r}. \qquad [80]$$

Since $\exp\{i\xi_{uv}(t, \Omega)\}$ is periodic, it may be written as a Fourier series:

$$\exp\{i\xi_{uv}(t, \Omega)\} = \sum_{k=-\infty}^{\infty} C_{uv}^{(k)}(\Omega)\exp\{ik\omega_r t\}. \qquad [81]$$

The signal component s_{uv} may also be written as a superposition of sidebands at frequencies $\omega_{uv}^{(0)}(\Omega) + k\omega_r$, with $\omega_{uv}^{(0)} = -\bar{\omega}_{uv}$:

$$s_{uv}(t, \Omega) = \sum_{k=-\infty}^{\infty} a_{uv}^{(k)}(\Omega)\exp\{i[\omega_{uv}^{(0)}(\Omega) + k\omega_r]t\}. \qquad [82]$$

By repeating the arguments in Refs. (*17*) and (*43*), it is possible to relate the γ-averaged signal component to the Fourier components $C_{uv}^{(k)}$:

$$\langle a_{uv}^{(k)}(\alpha, \beta)\rangle_\gamma = Z_{uv}|C_{uv}^{(k)}(\Omega)|^2. \qquad [83]$$

Since $\bar{\omega}_{uv}$ is independent of γ, this implies that the calculation of the signal may be reduced to a two-angle average over (α, β) of the functions $|C_{uv}^{(k)}(\Omega)|^2$.

The symmetries of $C_{uv}^{(k)}$ may now be established. From Eq. [74], omitting odd ranks L, the Hamiltonian eigenvalues have the symmetry

$$\omega_u(t, \Omega) = \omega_u(-t, \bar{\Omega}), \qquad [84]$$

which corresponds to the following relationships of the Fourier components for orientations Ω and $\bar{\Omega}$:

$$\omega_u^{(m)}(\Omega) = \omega_u^{(m)}(\bar{\Omega})^*. \quad [85]$$

This in turn leads to the following relationship of the ξ-functions

$$\xi_{uv}(t, \Omega) = -\xi_{uv}(-t, \bar{\Omega}), \quad [86]$$

and hence to the symmetries

$$C_{uv}^{(k)}(\Omega) = C_{uv}^{(k)}(\bar{\Omega})^*. \quad [87]$$

It follows that the γ-averaged signal components from orientations of the type (α, β) and $(\pi + \alpha, \pi - \beta)$ are identical:

$$\langle a_{uv}^{(k)}(\Omega)\rangle_\gamma = \langle a_{uv}^{(k)}(\bar{\Omega})\rangle_\gamma. \quad [88]$$

This proves the C_i-symmetry property in the case of a dynamically inhomogeneous interaction, with orientation-independent coherence preparation at the beginning of detection. This property applies independent of choice of reference frame.

We have recently shown that C_i symmetry also applies to several important classes of dynamically *homogeneous* problems, for example, the calculation of powder NMR spectra for arbitrary systems of coupled spins in rotating solids, in the absence of RF fields. Using the COMPUTE algorithm (*40*), a three-angle average may be reduced to a two-angle average over half of the sphere. This is discussed in a subsequent article (*34*).

In the case of a single interaction, or many interactions with the same principal axis frame, the frame M may be chosen to coincide with the principal axis frame. For even L interactions, this implies the symmetries

$$[A_{Lm}^{\Lambda}]^M = 0 \text{ for } m \text{ odd}$$
$$[A_{Lm}^{\Lambda}]^M = [A_{L-m}^{\Lambda}]^M. \quad [89]$$

The absence of molecular frame components with m odd leads immediately to the additional signal symmetry

$$s_{uv}(t; \alpha, \beta, \gamma) = s_{uv}(t; \pi + \alpha, \beta, \gamma). \quad [90]$$

The full D_{2h} symmetry may be recognized by considering the orientation defined $\Omega' = (-\alpha, \beta, -\gamma)$. From the symmetries of the principal axis frame tensors, and the Wigner function symmetry (*16*),

$$D_{mm'}^L(\Omega') = (-1)^{m'-m} D_{-m-m'}^L(\Omega), \quad [91]$$

one may demonstrate the following symmetry of the Hamiltonian Fourier components:

$$H_\Lambda^{(m)}(\Omega') = H_\Lambda^{(-m)}(\Omega). \quad [92]$$

This is analogous to Eq. [74], and the same reasoning may be followed to establish the following symmetry of the γ-averaged signals:

$$\langle a_{uv}^{(k)}(\Omega)\rangle_\gamma = \langle a_{uv}^{(k)}(\Omega')\rangle_\gamma. \quad [93]$$

The three properties of Eqs. [88], [90], and [93] establish together the D_{2h} symmetry of the γ-averaged MAS signal in this case.

The symmetry properties of NMR signals from static solids are much easier to establish since there is no intermediate reference frame R, and no γ dependence. The preceding equations may be used directly by setting $\beta_{\mathrm{RL}} = 0$. For example, Eq. [74] leads immediately to

$$H_\Lambda^{(0)}(\Omega_{\mathrm{ML}}) = (-1)^L H_\Lambda^{(0)}(\bar{\Omega}_{\mathrm{ML}}). \quad [94]$$

Since only the $m = 0$ Fourier component exists if $\beta_{\mathrm{RL}} = 0$, this property immediately establishes C_i symmetry for static solids if odd-spatial-rank interactions are ignored. It follows that orientational averaging over a hemisphere is almost always sufficient in static solids (*20*). The D_{2h} symmetry of static spectra in the case of a single interaction using the principal axis frame is also well known (*35*).

The preceding arguments were developed for the high-field limit. Second-order quadrupolar interactions are readily accommodated in the same framework by using a modified quadrupolar Hamiltonian which incorporates second-order shifts (*44*). Since all correction terms still have even L, the conclusions of this article are unchanged.

ACKNOWLEDGMENTS

This research was supported by the Swedish Natural Sciences Research Council and the Göran Gustafsson Foundation for Research in the Natural Sciences and Medicine. We acknowledge help from T. K. Hirsch in the early part of this project, N. D. Kurur, who informed us of the existence of the Lebedev schemes, and S. Dusold, Y. K. Lee, and O. N. Antzutkin for discussions. We thank C. Daul for providing us with some Lebedev angle sets and M. Bak and N. C. Nielsen for providing us with the REPULSION sets, as well as for constructive comments.

Note added in proof. Lebedev sets are now available up to $L_{\max}^{S} = 59$. (V. I. Lebedev, personal communication.)

REFERENCES

1. M. H. Levitt, D. P. Raleigh, F. Creuzet, and R. G. Griffin, Theory and simulations of homonuclear spin pair systems in rotating solids, *J. Chem. Phys.* **90,** 6347–6364 (1990).
2. T. Gullion and J. Schaefer, Rotational-echo double-resonance NMR, *J. Magn. Reson.* **81,** 196–200 (1989).
3. J. Heller, R. Larsen, M. Ernst, A. C. Kolbert, M. Baldwin, S. B. Prusiner, D. E. Wemmer, and A. Pines, Application of rotational

resonance to inhomogeneously broadened systems, *Chem. Phys. Lett.* **251,** 223–229 (1996).

4. Y. Ishii, T. Terao, and M. Kainosho, Relayed anisotropy correlation NMR: Determination of dihedral angles in solids, *Chem. Phys. Lett.* **265,** 133–140 (1996).
5. K. Schmidt-Rohr, Torsion angle determination in solid ^{13}C-labelled amino acids by SLF 2Q-NMR, *J. Am. Chem. Soc.* **118,** 7601–7603 (1996).
6. D. P. Weliky and R. Tycko, Determination of peptide conformations by 2D MAS NMR exchange spectroscopy with rotor synchronization, *J. Am. Chem. Soc.* **118,** 8487–8488 (1996).
7. X. Feng, Y. K. Lee, D. Sandström, M. Edén, H. Maisel, A. Sebald, and M. H. Levitt, Direct determination of a molecular torsional angle by solid-state NMR, *Chem. Phys. Lett.* **257,** 314–320 (1996).
8. I. Stewart, Crystallography of a golf ball, *Scientific American* **276,** 80–82 (1997).
9. V. I. Lebedev, Values of the nodes and weights of ninth to seventeenth order Gauss–Markov quadrature formulae invariant under the octahedron group with inversion, *Zh. Vychisl. Mat. Fiz.* **15,** 48–54 (1975).
10. V. I. Lebedev, Quadratures on a sphere, *Zh. Vychisl. Mat. Fiz.* **16,** 293–306 (1976).
11. V. I. Lebedev, Spherical quadrature formulas exact to orders 25–29, *Sibirsk. Mat. Zh.* **18,** 132–142 (1977).
12. V. I. Lebedev and A. L. Skorokhodov, Quadrature formulas of orders 41, 47 and 53 for the sphere, *Sov. Phys.—Dokl.* **45,** 587–592 (1992).
13. C. W. Murray, N. C. Handy, and G. J. Laming, Quadrature schemes for integrals of density functional theory, *Mol. Phys.* **78,** 997–1014 (1993).
14. O. Treutler and R. Alrichs, Efficient molecular integration schemes, *J. Chem. Phys.* **102,** 346–354 (1995).
15. C. Daul and S. Daul, Symmetrical ''nonproduct'' quadrature rules for a fast calculation of multicenter integrals, *Int. J. Quant. Chem.* **61,** 219–230 (1997).
16. D. A. Varshalovich, A. N. Moskalev, and V. K. Khersonskii, ''Quantum Theory of Angular Momentum.'' World Scientific, Singapore (1988).
17. M. H. Levitt, Why do spinning sidebands have the same phase?, *J. Magn. Reson.* **82,** 427–433 (1989).
18. J. Herzfeld and A. E. Berger, Sideband intensities in NMR spectra of samples spinning at the magic angle, *J. Chem. Phys.* **73,** 6021–6030 (1980).
19. T. Gullion and M. S. Conradi, Time symmetries in rotating sample NMR, *J. Magn. Reson.* **86,** 39–45 (1990).
20. D. W. Alderman, M. S. Solum, and D. M. Grant, Methods for analyzing spectroscopic line shapes. NMR solid powder patterns, *J. Chem. Phys.* **84,** 3717–3725 (1986).
21. M. J. Mombourquette and J. A. Weil, Simulation of magnetic resonance powder spectra, *J. Magn. Reson.* **99,** 37–44 (1992).
22. L. Andreozzi, M. Giordano, and D. Leporini, A fast algorithm for magnetic resonance lineshapes of powder samples, *J. Magn. Reson. A* **104,** 166–171 (1993).
23. D. Wang and G. R. Hanson, A new method for simulating randomly oriented powder spectra in magnetic resonance: The Sydney Opera House (SOPHE) method, *J. Magn. Reson. A* **117,** 1–8 (1995).
24. S. J. Varner, R. L. Vold, and G. L. Hoatson, An efficient method for calculating powder patterns, *J. Magn. Reson. A* **123,** 72–80 (1996).
25. M. Bak and N. C. Nielsen, REPULSION—A novel approach to efficient powder averaging in solid-state NMR, *J. Magn. Reson.* **125,** 132–139 (1997).
26. S. K. Zaremba, Good lattice points, discrepancy, and numerical integration, *Ann. Mat. Pura. Appl.* **4:73,** 293–317 (1966).
27. H. Conroy, Molecular Schrödinger equation. VIII. A new method for the evaluation of multidimensional integrals, *J. Chem. Phys.* **47,** 5307–5318 (1967).
28. V. B. Cheng, H. H. Suzukawa, and M. Wolfsberg, Investigations of a nonrandom numerical method for multidimensional integration, *J. Chem. Phys.* **59,** 3992–3999 (1973).
29. J. M. Koons, E. Hughes, H. M. Cho, and P. D. Ellis, Extracting multitensor solid-state NMR parameters from lineshapes, *J. Magn. Reson. A* **114,** 12–23 (1995).
30. L. González-Tovany and V. Beltrán-López, Second-order powder pattern and simulated spectra of EPR transitions in orthorhombic symmetry or NMR with quadrupolar interactions, *J. Magn. Reson.* **89,** 227–242 (1990).
31. W. H. Press, B. P. Flannery, S. A. Teukolsky, and W. T. Vetterling, ''Numerical Recipes in C. The Art of Scientific Computing.'' Cambridge Univ. Press, Cambridge, UK (1986).
32. B.-Q. Sun, J. H. Baltisberger, Y. Wu, A. Samoson, and A. Pines, Sidebands in dynamic angle spinning (DAS) and double rotation (DOR) NMR, *Solid State NMR* **1,** 267–295 (1992).
33. M. M. Maricq and J. S. Waugh, NMR in rotating solids, *J. Chem. Phys.* **70,** 3300–3316 (1979).
34. M. H. Levitt and M. Edén, *Mol. Phys.,* submitted.
35. C. P. Slichter, ''Principles of Magnetic Resonance.'' Springer-Verlag, Berlin (1990).
36. A. Llor and J. Virlet, Towards high-resolution NMR of more nuclei in solids: Sample spinning with time-dependent spinner axis angle, *Chem. Phys. Lett.* **152,** 248–253 (1988).
37. A. Llor, Z. Olejniczak, and A. Pines, Coherent isotropic averaging in zero-field nuclear magnetic resonance. I. General theory and icosahedral sequences, *J. Chem. Phys.* **103,** 3966–3981 (1995).
38. A. Llor, Z. Olejniczak, and A. Pines, Coherent isotropic averaging in zero-field nuclear magnetic resonance. II. Cubic sequences and time-reversal of spin couplings, *J. Chem. Phys.* **103,** 3982–3997 (1995).
39. G. Strang, ''Linear Algebra and Its Applications.'' Harcourt Brace Jovanovich, San Diego (1988).
40. M. Edén, Y. K. Lee, and M. H. Levitt, Efficient simulation of periodic problems in NMR. Application to decoupling and rotational resonance, *J. Magn. Reson. A* **120,** 56–71 (1996).
41. O. N. Antzutkin and M. H. Levitt, Centerband phase shift in the TOSS spectra of a magic-angle-spinning single crystal, *J. Magn. Reson. A* **118,** 295–298 (1996).
42. P. Hodgkinson and L. Emsley, The reliability of the determination of tensor parameters by solid-state NMR, *J. Chem. Phys.* **107,** 4808–4816 (1997).
43. O. N. Antzutkin, S. C. Shekar, and M. H. Levitt, Two-dimensional sideband separation in magic-angle-spinning NMR, *J. Magn. Reson. A* **115,** 7–19 (1995).
44. A. Samoson, E. Kundla, and E. Lippmaa, High resolution MAS-NMR of quadrupolar nuclei in powders, *J. Magn. Reson.* **49,** 350–357 (1982).